

See discussions, stats, and author profiles for this publication at: <https://www.researchgate.net/publication/365185274>

Flow and heat transfer studies of multijet impingement cooling for different configurations: A review

Article in Heat Transfer · November 2022

DOI: 10.1002/htj.22757

CITATION

1

READS

689

2 authors:



Babji Gudla

Independent Researcher

12 PUBLICATIONS 41 CITATIONS

[SEE PROFILE](#)



Arun Kumar Pujari

INDIAN INSTITUTE OF PETROLEUM AND ENERGY

21 PUBLICATIONS 77 CITATIONS

[SEE PROFILE](#)

Flow and heat transfer studies of multijet impingement cooling for different configurations: A review

Gudla Babji  | Arun Kumar Pujari

Department of Mechanical Engineering,
Indian Institute of Petroleum & Energy,
Visakhapatnam, Andhra Pradesh, India

Correspondence

Arun Kumar Pujari, Department of
Mechanical engineering, Indian Institute
of Petroleum and Energy, 2nd Floor
AUCE Main Building, Siripuram,
Vishakhapatnam 530003,
Andhra Pradesh, India.
Email: arun.pujarimec@iipe.ac.in

Abstract

Increasing the gas turbine engine's turbine intake temperature has long been a potential strategy for increasing the specific work output of the engine. However, the melting temperature of the turbine blades and vane material limits the maximum intake temperature. As a result, internal and external cooling techniques are commonly used to maintain the vane material in a safe condition. This study provided an overview of internal impingement cooling to highlight the significance of geometrical variations, such as flat plate, curve plate, and actual vanes. It was observed that flat and curved plate impingement heat transfer studies were reported extensively, whereas limited studies were found on the conjugate effects on airfoil surfaces. The importance of conjugate heat transfer studies and their impact has recently been described in the literature. In most of the literature, a wide range of instruments, such as Laser Doppler Velocimeter, Particle Image Velocimeter, liquid crystal sheets, and so forth, were used for experimental investigations. According to most studies, the local value of internal surface temperature and heat transfer coefficient are vital factors of local flow behavior. Jet-to-jet spacing, jet-to-plate spacing, jet hole diameter, and jet Reynolds

Abbreviations: HTC, heat transfer coefficient; NDT, nondimensional temperature, θ ; NGV, nozzle guide vane; RANS, Reynolds Averaged Navier Stokes; SST, shear stress transport.

numbers played a crucial role in both numerical and experimental analyses. Different geometric variations strongly influence flow behavior. Therefore, the usual method for determining interior temperature distributions and heat transfer coefficients by considering generalized geometries like the flat and curved plate may not produce accurate conjugate solutions. Most of the computational studies on the flat and curved plate indicate the usage of $\kappa-\omega$ shear stress transport and $\kappa-\varepsilon$ realizable model to predict the heat transfer coefficient.

KEY WORDS

combined impingement, film cooling, heat transfer, impingement cooling, literature review

1 | INTRODUCTION

Current advanced gas turbines operate at a higher inlet temperature to yield high efficiency and specific work output. The ever-increasing demand for higher gas turbine inlet temperatures is limited by the allowable thermomechanical stresses induced in their vanes and blades. The safe upper limit of temperature can be enhanced by using novel material composition and adopting appropriate cooling technologies. In this process, the material properties and the cooling configuration should be chosen so that the surface temperature of the blade is kept low and uniform while consuming as little cooling air as possible. As the turbine blades are cooled with the high-pressure air extracted from the compressor, it is necessary to fully understand the flow and thermal characteristics of various cooling configurations and use this knowledge to optimize the related parameters.

Gas turbine blades are cooled both from the internal and external sides. Internal cooling techniques include impingement, pin fin, and convective cooling over augmented surfaces to enhance heat transfer. The effusion or film cooling prevents the external surface from receiving large quantities of heat from the hot mainstream. Among the above-mentioned internal cooling techniques, impingement cooling provides the maximum localized heat transfer rate by allowing the fluid to impinge on the hot surface. The impingement cooling in a gas turbine blade/vane can be achieved by multiple air jets. When allowed to pass through small diameter nozzles or orifices, the coolant comes out as high-velocity jets. When a high-velocity jet strikes the interior surface of the vane, it results in a high heat transfer rate between the surface and the coolant. This method of cooling is called jet impingement cooling. A figure combining the flow features of multiple jet impingements is shown in Figure 1.

The coolant has a uniform velocity profile at the nozzle exit for low-diameter small jet orifices. However, as the coolant advances towards the target surface, the outer layer of the jet broadens due to continuous entrainment and momentum exchange with the surrounding fluid. Consequently, the inner zone with the potential core (where the uniform velocity is maintained) shrinks. This region of jet flow that remains unaffected by the impinging surface is termed the free jet region. The free jet region is thus characterized by the central potential

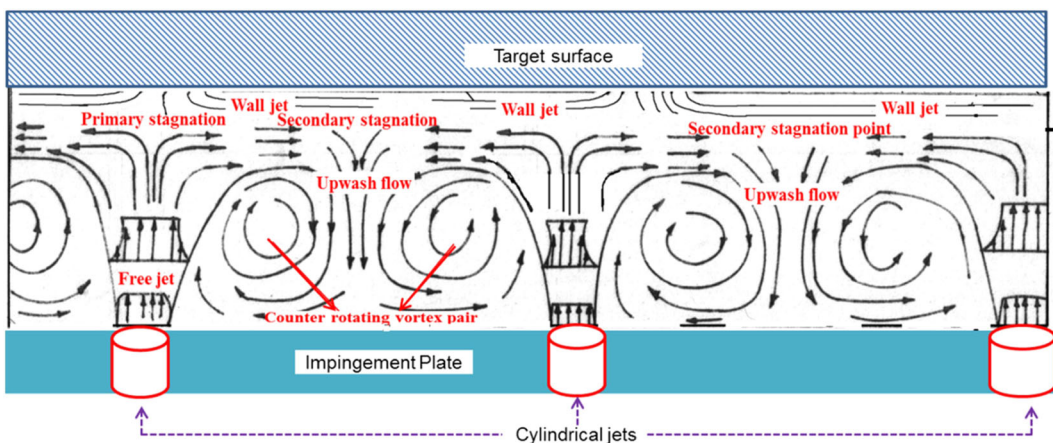


FIGURE 1 Different flow regimes for cooling with multiple jet impingements¹ [Color figure can be viewed at wileyonlinelibrary.com]

core and the low-velocity shear layer that results from the entrainment of the surrounding fluid into the jet. The impingement or stagnation zone is where the jet makes contact with the surface. From this location, the flow is accelerated in the direction parallel to the plate. Due to continuous entrainment of the surrounding fluid, the acceleration is not sustained downstream but gets transformed into a decelerating flow over the surface. This region is termed the wall jet. A secondary stagnation zone is formed when one wall jet encounters another belonging to the neighboring jet. In the case of multijet impingement cooling, this region is named the upwash region. In the upwash region, the wall jets, after mutual interactions, move upward, and act as a fountain. The interaction between the fluid in the fountain and the main jet promotes entrainment. This phenomenon dramatically depends upon the jet-to-jet spacing (pitch), the jet (nozzle) to (the target) plate spacing (H), and the geometry of the target surface. The above flow features result in a very high heat transfer coefficient in the stagnation zone, followed by a decreasing trend in the wall jet region. Heat transfer again increases in the secondary stagnation region. The impingement surface's heat transfer pattern further depends on how the spent air is removed from the domain.

The addition of film-cooling holes significantly alters the behavior of impinging jets and is referred to in the literature as combined impingement and film cooling. The combined impingement and film cooling are very effective ways of keeping the blade temperature within safer limits. The high-velocity coolant impinges on the vane's internal surface and exits through the film holes, forming a film on the vane's exterior surface. The flow and heat transfer characteristics observed in a traditional jet impingement or film-cooling configuration differ from those observed in combined multiple impingements and film-cooling arrangements. Numerous geometric and flow variables affect the thermofluid dynamic properties of the combined hybrid cooling setup. Some of these variables are (i) the shape of the coolant plenum chamber, (ii) the shape and size of holes transporting the coolant, (iii) the spacing between the target plate to impinging jet where the impingement takes place, (iv) the geometric configuration of the target surface (after impinging upon the target surface how the coolant flow over the surface), (v) the location and shape of the film-cooling hole, (vi) the hot mainstream pressure gradient effect over the surface, (vii) the film coolant interaction with the mainstream flow (depending upon the film holes inclination), and (viii) the blade material conductivity, influenced by the external film resistance and internal convective resistance.

The cooled blade designs, which are aimed at uniform temperature distribution within the blade, are thus dependent on these essential geometric, flow, and thermal variables. The geometric and flow variable that may prevail in a flat plate with impingement and film cooling is presented in Figure 2. The external flow and heat transfer behavior in the case of a gas turbine vane/blade may vary considerably compared with the flat plate studies. Figure 3 illustrates the impingement and film coolant flow characteristics in the chordwise direction. The variable color of the flow lines indicates the variation of thermofluid dynamic factors that affect the heat transfer phenomena.

As jet impingement cooling is the most promising internal cooling method, the literature on the flow and heat transfer for impinging jet configurations is discussed for various geometric profiles, such as flat plate, curved plate, and other geometries. The objective of the present study is to briefly explain the available literature related to the flow and heat transfer characteristics of the jet impingement and combined impingement with other external cooling methods for different configurations. Also, to represent the variations between the experimental and numerical results, to present the significance of the conjugate effect. The importance of the aerofoil surface study rather than flat and curved plates is demonstrated. Suitable computational methods for the analysis to obtain accurate results are suggested based on previous literature studies.

Some representative papers are briefly discussed to highlight the essential flow features associated with jet impingement cooling. In this context, the flow and heat transfer characteristics of impinging jets are grouped under the following heading

- Flow and heat transfer studies of impinging jets on a flat plate,
- Flow and heat transfer studies of impinging jets on a curved plate,
- Conjugate heat transfer studies on airfoil-shaped blades.

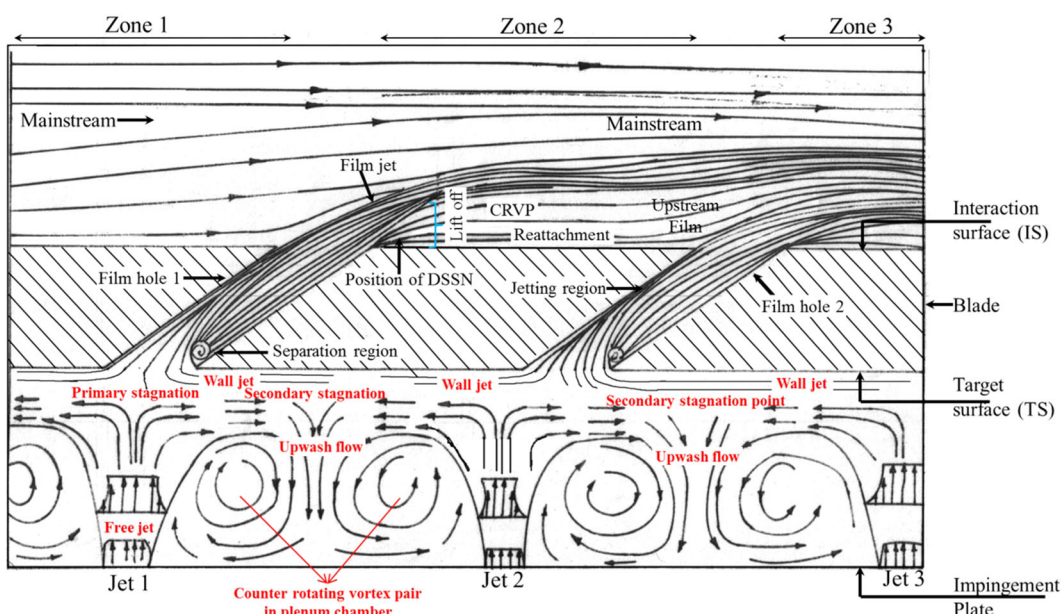


FIGURE 2 Different flow regions for a combined impingement and film cooling for a flat plate¹ [Color figure can be viewed at wileyonlinelibrary.com]

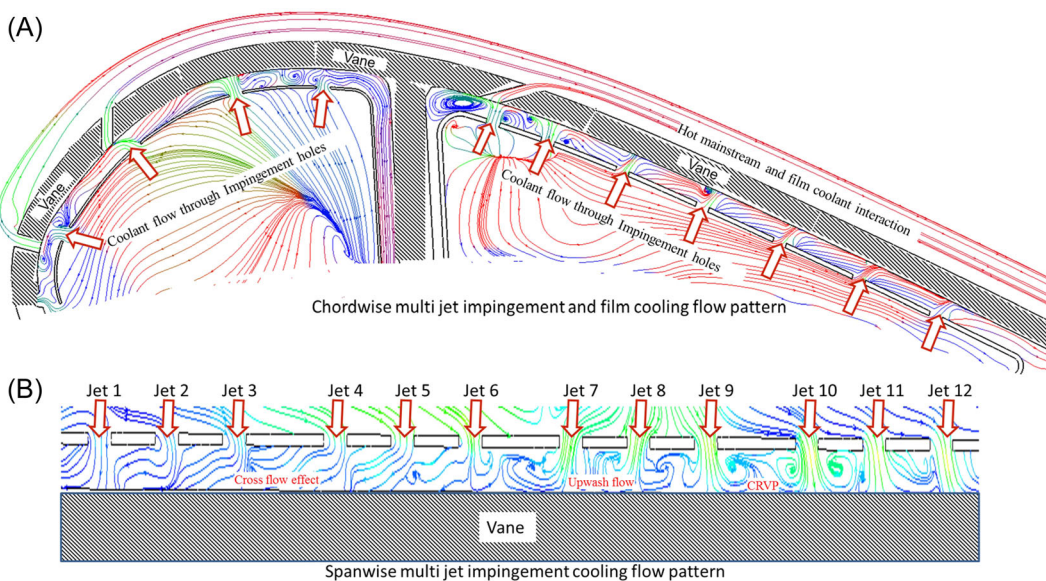


FIGURE 3 Flow structure for a combined impingement and film cooling for a vane surface¹ [Color figure can be viewed at wileyonlinelibrary.com]

2 | FLOW AND HEAT TRANSFER STUDIES OF IMPINGING JETS ON FLAT PLATE

2.1 | Flow and heat transfer studies of single jet impinging on the flat plate

The effects of confinement and the cross-flow have been brought out to resemble the actual internal flow closely. The studies on impingement cooling where the flow is unconfined are studied as free jets. Such studies are omitted from the present “internal cooling” discussion. Some representative papers are briefly discussed to highlight the important flow features associated with jet impingement cooling.

2.1.1 | Flat plate with single confined impinging jets

Jambunathan et al.² evaluated the heat transfer characteristics of single circular impinging jets on a flat surface. They investigated the influence of (a) nozzle geometry on heat transfer characteristics and (b) inlet turbulence (nozzle-to-plate spacing). While presenting the correlations for the Nusselt number for an unconfined impinging jet heat transfer, they pointed out from the available data on a flat plate that confinement causes a reduction in heat transfer rates. They concluded that the Nusselt number is independent of nozzle-to-plate spacing up to 12 nozzle diameters at radii higher than six nozzle diameters from the stagnation point. The outcomes of a simple extrapolation for calculating wall jet heat transfer coefficients compare in line with reported data.

Al-Sanea³ quantitatively investigated the heat transfer properties of laminar slot jets impinging on an isothermal flat surface in three distinct instances: (a) free jet impingement,

(b) semiconfined jet impingement, and (c) semiconfined jet impingement with cross-flow. Additionally, they conducted detailed parametric research on the Reynolds number of jets, fluid Prandtl number, length of the heat transfer surface, and jet exit to impingement surface distance. They reported that free and semiconfined jet impingement shows practically identical results near the impingement region and a slight difference found away from the jet impingement region. Additionally, they discovered that cross-flow impairs the beneficial properties of impinging jets and decreases the Nusselt number.

San et al.⁴ determined the local Nusselt number of a circular confined air jet on a flat jet, allowing the limited jet flow to move in two opposing directions. They maintained a consistent heat flux for various jet diameters and altered the jet Reynolds number between 30,000 and 67,000 while retaining a constant target plate distance to jet diameter ratio ($H/d = 2$). They discovered a correlation between the Nusselt number and the confined jet that is proportional to the 0.6375 power of the Reynolds number. They concluded that a more minor jet hole diameter results in a lower Nusselt number for a constant Reynolds number. Additionally, they noted that surface heat flux might become a factor marginally altering the Nusselt number for constrained jet impingement heat transfer.

Fitzgerald and Garimella⁵ experimentally studied the effects of axisymmetric, confined, and submerged turbulent jets that were normally impinged on a flat plate using laser doppler velocimetry. They conducted experiments with two different nozzle diameters for a range of Reynolds numbers (8500–23,000). They noticed a toroidal recirculation pattern in the confined jet's outflow zone. The location of the toroid moved radially outward with an increase in Reynolds number and nozzle-to-target plate spacing shown in Figure 4 for a nozzle diameter of 6.35 mm at a height-to-diameter ratio of 3.

Behnia et al.⁶ used an elliptic relaxation turbulence model to investigate the influence of turbulent heat transfer in confined and unconfined impinging jets ($v^2 - f$ model). They found findings for a variety of Reynolds numbers and jet-target distances. They stated that confinement decreases average heat transfer rates but does not affect the local stagnation heat transfer coefficient. They concluded that confinement considerably affects the small nozzle-to-plate distances ($H/d < 0.25$). Figure 5 shows the contours of turbulence kinetic energy for the two models ($\kappa-\epsilon$ and $v^2 - f$ models). $v^2 - f$ model predicted more accurately compared with the $\kappa-\epsilon$ model.

Li and Garimella⁷ investigated the effect of fluid thermophysical properties on heat transfer from impinging jets that are confined and submerged. They conducted experiments using different fluids, like, air, water, and fluorine (FC-77) and obtained a correlation between stagnation and area-averaged Nusselt number. They found a higher magnitude of heat transfer coefficient with water jets. Koseoglu and Baskaya⁸ have studied the flow field of confined circular and elliptic jets experimentally using Laser Doppler anemometry (LDA). Their results show that for confined circular and elliptical geometries, the inner peaks in local heat transfer coefficients closely relate to the turbulence intensities in the jet and radial flow acceleration along the wall. Figure 6 shows the velocity distributions obtained from LDA close to the jet centreline for the circular and elliptical jet at H/d ratios 2 and 6 for $Re = 10,000$. High spreading rates were observed along the minor axis compared with the major axis and circular jets for both H/d ratios.

Kozlov et al.⁹ conducted experiments to study the influence of initial conditions at the nozzle exit of a round jet and reported that the nozzle length must be increased over a specific value to provide for spatial growth of turbulent boundary layer thickness.

Alekseenko et al.¹⁰ analyzed high-swirl turbulent jet by using the tomographic particle image velocimetry technique and processed by the proper orthogonal decomposition (POD)

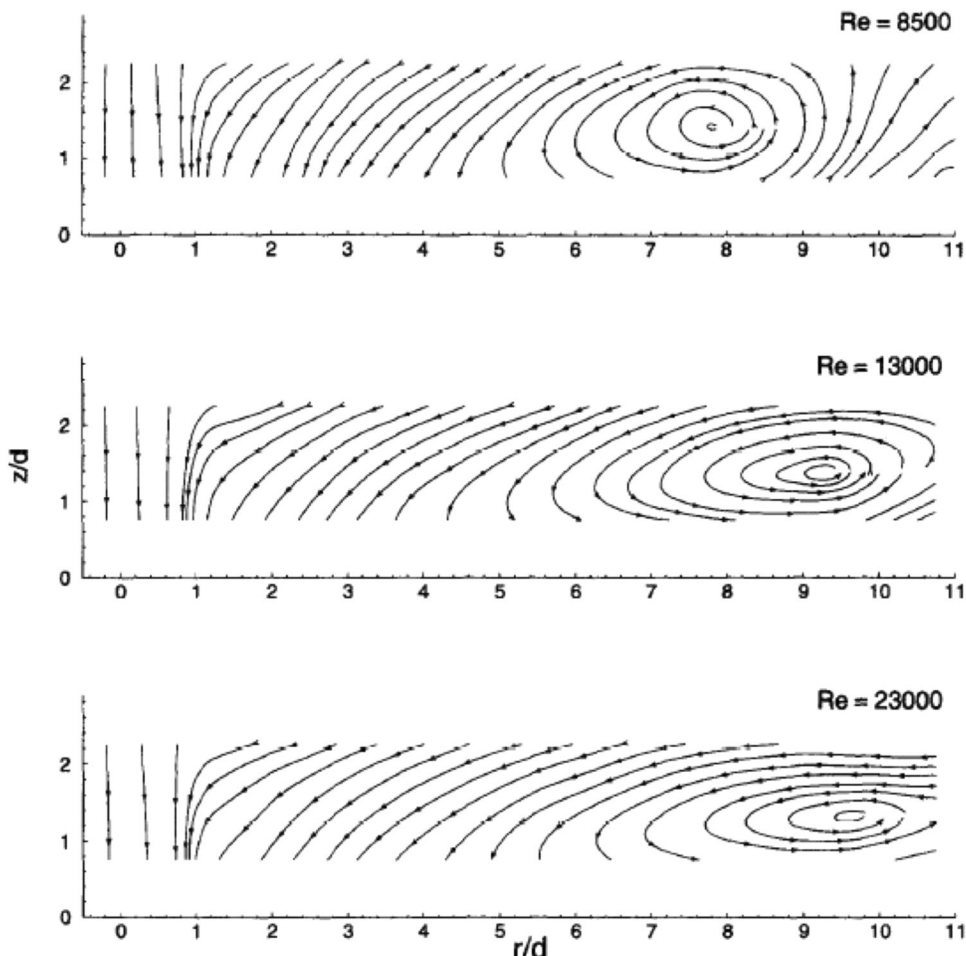


FIGURE 4 Recirculating flow patterns for $d = 6.35$ mm and $H/d = 3$ at $Re = 8500, 13,000$ and $23,000$ ⁵

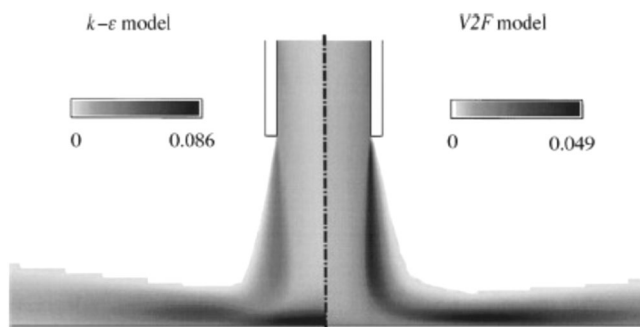
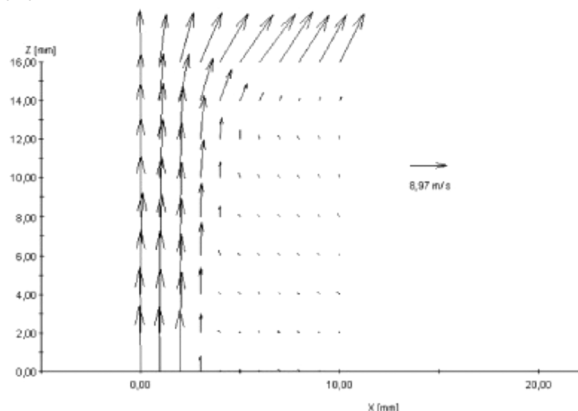
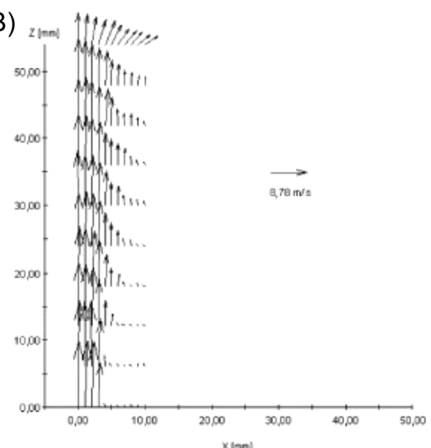


FIGURE 5 Shaded contours of turbulence kinetic energy for the impinging jet on a flat plate $H/d = 2$ and $Re = 23,000$ ⁶

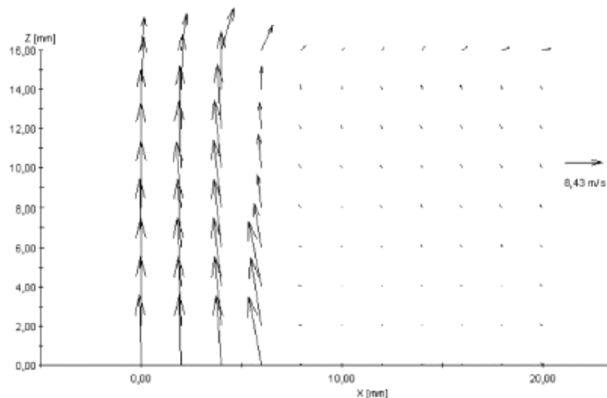
(A)



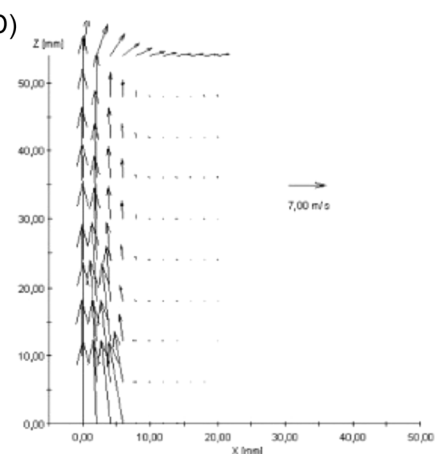
(B)



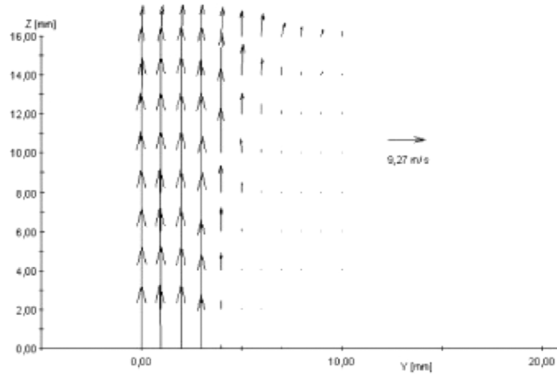
(C)



(D)



(E)



(F)

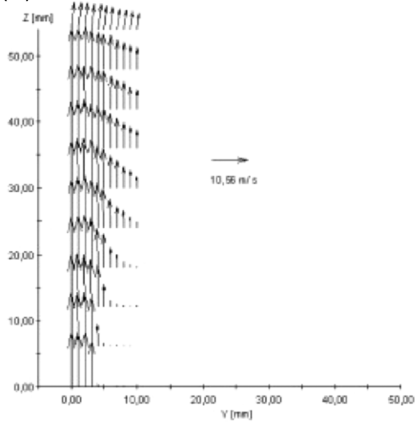


FIGURE 6 LDA velocity vector distribution near the jet center line for (A) circular jet $H/d = 2$, (B) circular jet $H/d = 6$, (C) major axis elliptical jet $H/d = 2$, (D) major axis elliptical jet $H/d = 6$, (E) minor axis elliptical jet $H/d = 2$, and (F) minor axis elliptical jet $H/d = 6$ ⁸

method and found that the detected intensive coherent velocity component corresponding to a helical vortex core of the swirling jet and two secondary spiral vortices. The entire coherent structure was rotating around the jet axis in compliance with the direction of the flow swirl.

Firdaus et al.¹¹ experimentally investigated the effectiveness of jet impingement on a flat plate at different conditions, such as different nozzle-to-plate distance, type of flow (laminar or turbulent), and various surface roughness. Surface roughness was changed by using other materials, zinc, aluminum, and mild steel. Mild steel (high surface roughness) was not suitable for jet impingement at turbulent flow but was ideal for laminar flow. The best impingement cooling system that could be obtained was a dimensionless nozzle to surface distance of 10 and a mass blow rate of 8.4 m/s using less surface roughness material (zinc). The summary of literature including the method of investigation, and techniques used both experimental and numerical are tabulated as shown in Table 1.

2.2 | Flow and heat transfer studies of multiple jets impinging on a flat plate

2.2.1 | Flat plate with cross-flow effect

Multiple jets are used for impingement cooling different regions of the nozzle guide vane interior. To simplify the analysis, a small portion of the midchord region of the vane surface is considered a flat plate, and heat transfer analysis was carried out extensively by many previous researchers.

Florschuetz et al.¹² investigated two-dimensional arrays of circular air jets impinging on a parallel to the jet orifice plate heat transfer surface. They created an arrangement of initial cross-flow through an upstream extension of the channel to replicate the impingement-cooled midchord section of a gas turbine airfoil. In most cases, they found that the addition of initial cross-flow resulted in reduced mean values of the Nusselt number.

Jakubowski¹³ experimentally studied the interaction of multiple jets by injecting twin jets normal to a cross-flow. They presented turbulence data from hot wire anemometry. They concluded that the mean velocities and Reynolds stress for the single and tandem jets show very similar behavior, indicating that the exact mechanism causes the turbulent nature of jets.

Van Treuren et al.¹⁴ noticed that at the beginning of the array of jets, where the cross-flow was small, the peak in Nusselt number was located at the hole centerline, and as the cross-flow developed with the downstream distance, the peak position shifted downstream. They mentioned that when the heat transfer pattern on the impingement surface was circular, it indicated that cross-flow had little effect. Brizzi et al.¹⁵ studied jets' aerodynamic and thermal behavior impinging on a plain wall. Their LDA measurements showed that the interaction between two neighboring jets creates a flow detachment along the periphery of each impingement zone, provoking the formation of vortices. Their study also revealed the cellular aspects of flow near the impingement wall and the presence of detachment and reattachment lines in frontier zones between different cells.

Hwang and Cheng¹⁶ experimented by varying the outflow orientation and found that the local heat transfer coefficient was significantly affected by the outflow orientation. Ekkad et al.¹⁷ investigated the effects of cross-flow and impingement on coolant flow inside a two-pass coolant channel, where impingement and passage cross-flow was generated by a dividing wall having a series of straight and inclined holes. They considered three different lateral hole

TABLE 1 Summary of literature on single jet impinging on a flat surface

Authors and year	Geometry	Parameters considered	Method of investigation	Technique used	Remarks
Al-Sanea (1992) ³	Flat surface with (a) free jet impingement, (b) semiconfined jet impingement, and (c) semiconfined jet impingement with cross-flow	Jet Reynolds number: 50–450; Prandtl number: 0.1–100; Length of heat transfer surface: 6.5–20; Jet-to-plate spacing: 1–16	Computational	Finite difference method, computer program	Free and semiconfined jet impingement shows practically identical results near the impingement region and slightly different from the jet impingement region
San et al. (1997) ⁴	Flat surface with a confined single jet	Jet Reynolds number: 30,000–67,000; Jet diameter: 3, 4, 6, and 9 mm; Jet-to-plate spacing: 2	Experimental	Turbine flowmeter	Smaller jet hole diameters have a lower Nusselt number for a constant Reynolds number
Fitzgerald and Garimella (1998) ⁵	Flat surface with a confined and submerged single jet	Jet Reynolds number: 8500–23,000; Jet diameter: 3.18 and 6.35 mm; Jet-to-plate spacing: 4	Experimental	Laser Doppler Velocimeter	Mentioned the toroidal recirculation pattern in the outflow region for the confined jet and its movement in the radially outward direction with an increase in Reynolds number and nozzle-to-target plate spacing
Behnia et al. (1999) ⁶	Flat surface with single jet; as free jet as well as confined jet	Jet Reynolds number: 23,000; Jet-to-plate spacing: 2, 0.5, and 0.25	Computational	Elliptic relaxation turbulence model	Confinement leads to decreased average heat transfer rates, but the local stagnation heat transfer coefficient is unchanged. They concluded that the effect of confinement is very significant for the low nozzle-to-plate distances ($H/d < 0.25$)

TABLE 1 (Continued)

Authors and year	Geometry	Parameters considered	Method of investigation	Technique used	Remarks
Li and Garimella (2001) ⁷	Flat surface with single jet for confined and submerged case	Jet Reynolds number: 4000–23,000; Jet diameter: 1.59, 6.35, and 12.7 mm; Jet-to-plate spacing: 1–4	Experimental	Foil-type heater and orificemeter	Obtained correlation for stagnation and area-averaged Nusselt number. They found a higher magnitude of heat transfer coefficient with water jets
Koseoglu and Baskaya (2008) ⁸	Flat surface with a confined single jet	Two different nozzle geometries: (i) circular and (ii) elliptical; Jet Reynolds number: 10,000; Jet-to-plate spacing: 2 and 6	Experimental	Laser Doppler Anemometer	The inner peaks in local heat transfer coefficients closely relate to the turbulence intensities in the jet and radial flow acceleration along the wall
Aleksenko et al. (2016) ¹⁰	Flat surface with high turbulence swirling jet	Swirling jet with vortex core breakdown; Nozzle diameter: 15 mm	Experimental	Tomographic particle image velocimeter	A helical vortex core of the swirling jet and two secondary spiral vortices are observed
Firdaus et al. (2019) ¹¹	Flat surface of different roughness with single impinging jet	Jet-to-plate distance: 5, 10, and 15; Material of flat plate: Zn, Al, Mild steel; Mass blow rates 4.5, 8.4, and 12.8 m/s	Experimental	Surface roughness tester, anemometer	Less surface roughness material (Zn) is suitable for impingement system

configurations for which they varied the Reynolds number ($Re = 10,000\text{--}50,000$). Their observation concluded that coolant supply from one channel to another inside the blade appears more promising than conventional U-bend serpentine channel design. Another important statement from their study was the need for a rib turbulator on the second pass may be eliminated due to significantly higher heat transfer enhancements using lateral injection configurations.

2.2.2 | Flat plate with different geometry holes of impinging jets

Son et al.¹⁸ investigated a large-scale model of a realistic impingement cooling system for an engine, where they carried out several tests to characterize impingement jet behavior fully. They observed that the shape of heat transfer distribution under each jet at the beginning of the impingement plate was circular. However, these shapes were larger and distorted in the exit part due to the high cross-flow effect. Due to the sudden deceleration of flow, the decline in the Nusselt number was more significant on the upstream side of the stagnation point than on the downstream side.

Aldabbagh and Sezai¹⁹ used the projection of flow lines to explain impinging square jets' flow and heat transfer behavior. The peripheral vortices around the jet and upwash flow at the collision point of the jets were seen for H/d cases above 0.25. For $H/d = 0.25$, no upwash fountain was formed because the wall jets filled the entire plate-to-plate spacing. Detailed flow lines were shown in Figure 7. However, the magnitude of the maximum Nusselt number remained unaffected. Jet-to-plate heat transfer has a significant effect on heat transfer. The spacing of jet-to-plate revealed a complicated flow environment with peripheral vortex forms surrounding each jet and an upwash-fountain flow at the jets' collision location. The nozzle determines any peripheral vortex's size and placement to plate spacing. The square jet configuration with Nu number variation for different jet-to-plate distances is shown in Figure 8.

The effect of impingement hole arrangements on flow and heat transfer was reported by Thielen et al.²⁰ Two configurations were used: a square configuration (3×3 evenly spaced jets) and a circular configuration (eight jets surrounding a central jet). Except for the center jet, the separate jets in the circular design showed similar heat transmission characteristics. At the same time, square jets showed much difference between the jets and high heat transfer rates for some of the jets due to the asymmetric flow field.

Yan et al.²¹ studied the Reynolds number effect of elliptic jets for three different exit flow configurations. They noticed aspect ratio and cross-flow significantly influenced the axial shift of impingement locations. They concluded that the two-way exit flow condition is most beneficial to the heat transfer characteristics of an impinging jet array.

Geers et al.²² investigated the velocity field and turbulent fluctuations within a hexagonal array of circular jets impinging on a planar wall. Their measurements indicate that the combination of self-induced cross-flow and wall jets resulted in the production of a system of horseshoe-shaped vortices surrounding the array's outer jets. They also reported that the center jet has the shortest core and highest turbulent kinetic energy because of the influence of neighboring jets.

Chambers et al.²³ examined the cooling performance of a 19-holed narrow impingement channel. Figure 9 shows the impingement channel geometry. They investigated the effect of initial cross-flow on jet penetration using a novel test technique. They conducted trials at a Reynolds number characteristic of an engine (20,000) and concluded that cross-flow strongly

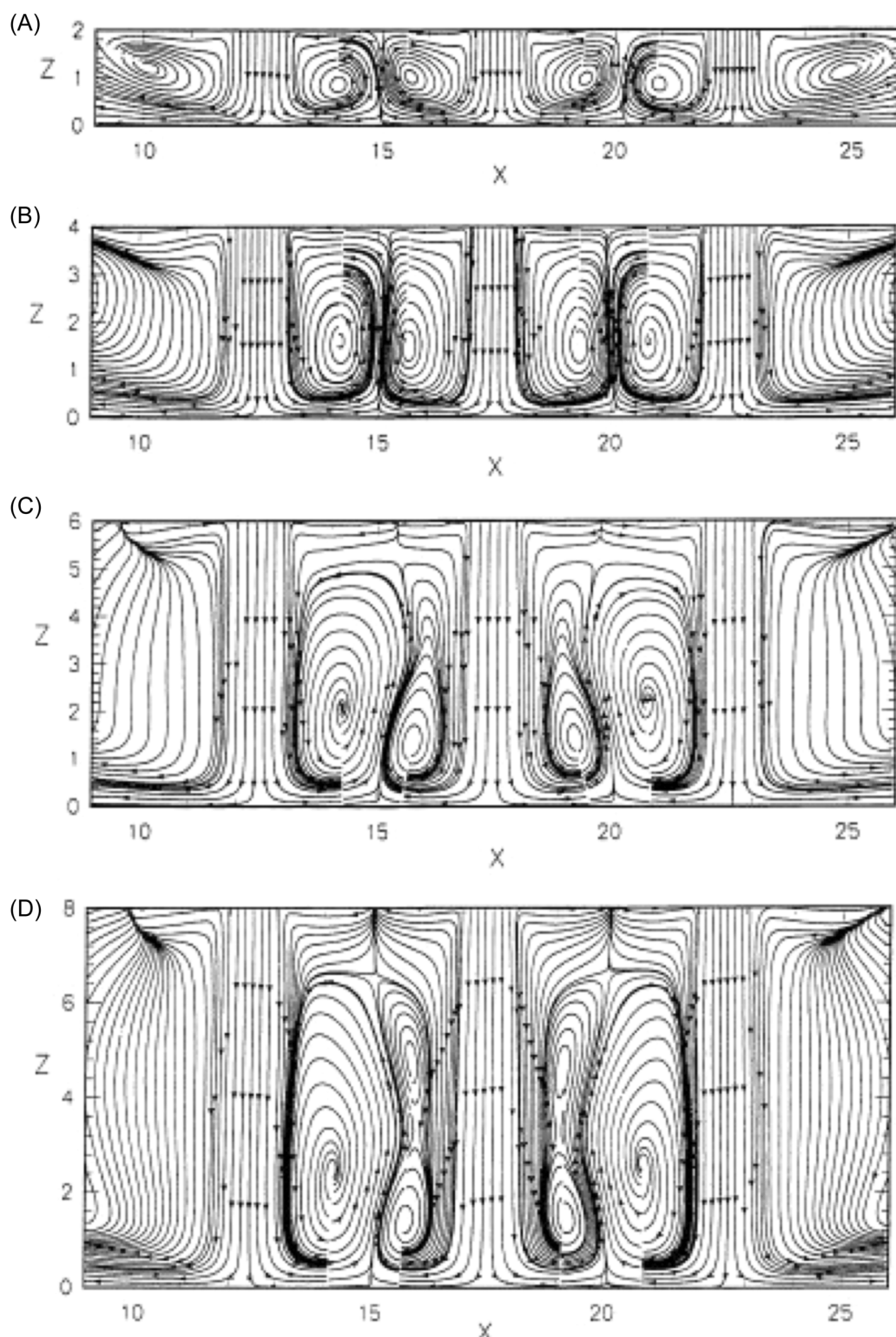


FIGURE 7 Projection of flow lines along the mid- x - z -axis for $Re = 100$ at the jet-to-plate spacing: (A) 2, (B) 4, (C) 6, and (D) 8^{19}

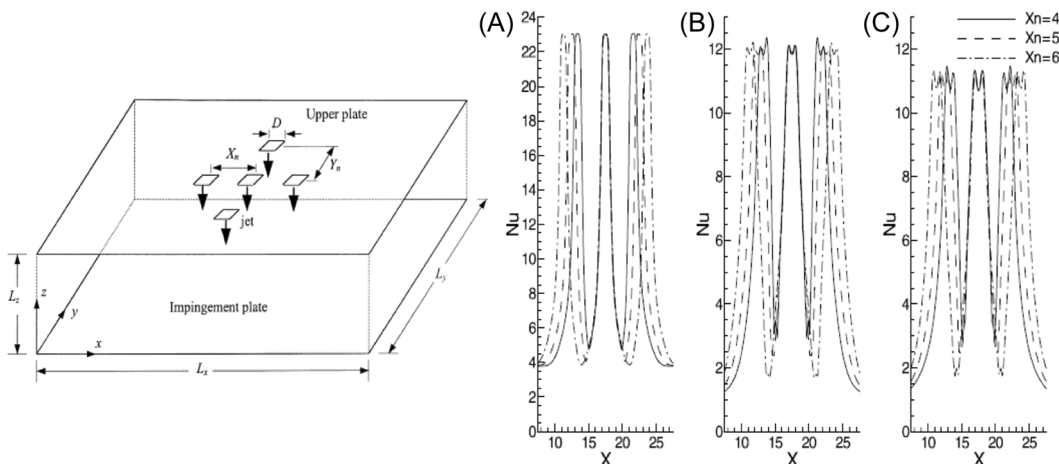


FIGURE 8 Definition of geometrical parameters (left) Nu number variation for jet-to-plate space ratios: (A) 0.25, (B) 1, and (C) 2 (right)¹⁹

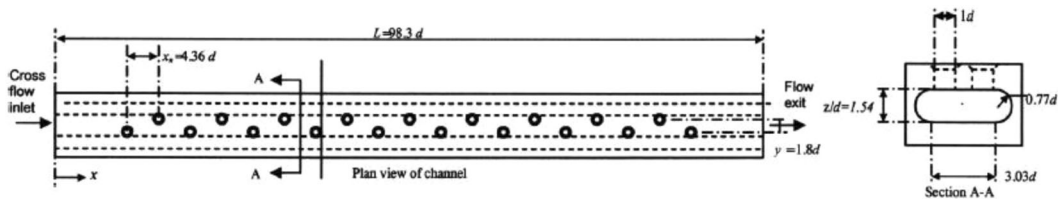


FIGURE 9 Impingement channel geometry²³

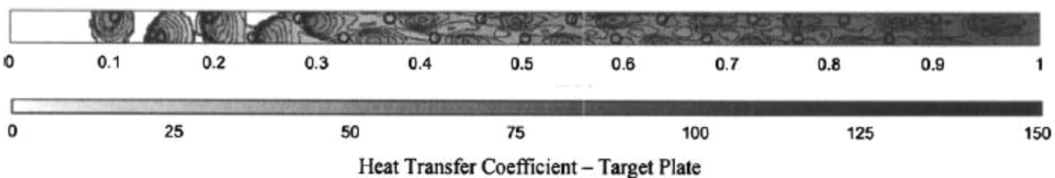
influences the heat transfer behavior. They reported that a 10% increase in initial cross-flow could diminish the mean effectiveness of target plates by 57%. This can be observed in Figure 10.

2.2.3 | Flat plate with different geometry holes of impinging jets

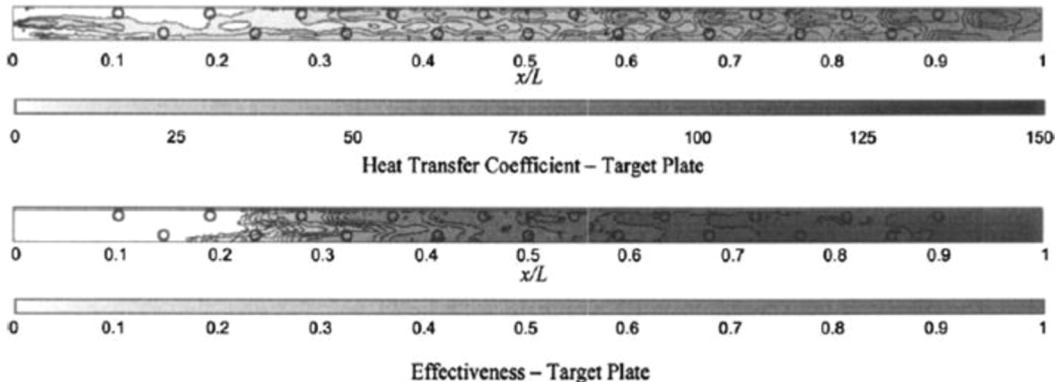
The effects of nozzle geometry (circular and cusped ellipse) and thermal boundary conditions (isothermal surface and uniform heat flux) on the flow and heat transfer characteristics of a semiconfined impinging jet were investigated by Dano et al.²⁴ Higher heat transfer for the circular jet was obtained for the isothermal case. In uniform heat flux cases, cusped elliptical geometry yielded higher heat transfer.

Goodro et al.²⁵ investigated the impact of jet impingement heat transfer on the Mach and Reynolds numbers. They obtained discharge coefficient, local and spatially averaged Nusselt numbers, and recovery factors for two sets of cases: (a) for a range of Mach numbers at constant Reynolds number and (b) for a range of Reynolds numbers at constant Mach number. They developed a correlation equation for the spatially averaged Nusselt number at a higher Mach number (0.74) that had not before been published. Local Recovery factor data are higher below in the regions of impact locations of the impinging jets, with values as large as 1.03 in the range of Mach number 0.74 and Reynolds number 60,000.

(A)



(B)



(C)

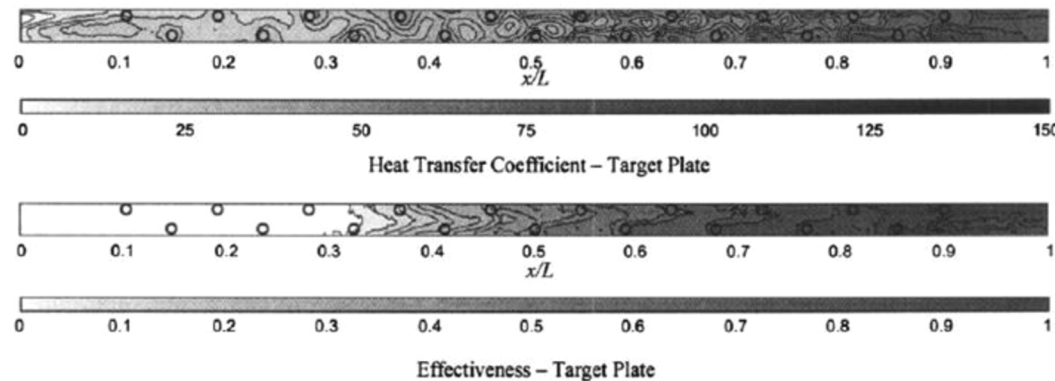


FIGURE 10 Heat transfer coefficient and effectiveness for target plate at $Re = 20,000$: (A) no cross-flow (no effectiveness), (B) 5% cross-flow, and (C) 10% cross-flow²³

Xing et al.²⁶ examined the heat transfer properties of impinging jet arrays inline and staggered arrays due to the low level of cross-flow at the upstream end of the plate, and the heat transfer peak was positioned at the jet centerline. On the downstream side of the plate, the peak location was displaced downstream due to the formation of cross-flow. In the downstream zone, the inline pattern was preferable to the staggered pattern because the inline pattern shielded the jets from the oncoming cross-flow. On the other hand, the cross-flow influenced the jets more directly for the staggered pattern. The heat transfer was enhanced with the staggered arrangement because of the impingement cooling and the high cross-flow convective heat transfer.

Chambers et al.²⁷ described a computational and experimental analysis of shaped elliptical impingement holes meant to enhance impinging jet penetration over a coolant route, which is

advantageous in areas with substantial cross-flow. They detected a 16% increase in the Nusselt number on the impingement target surface in the cooling passage's downstream half.

Xing and Weighard²⁸ considered a nine-by-nine inline jet array to examine the optimum jet-to-plate spacing. They changed the target plate distance to the jet diameter ($H/d = 1, 2, 3, 4$, and 5) used for three different cross-flow schemes, namely, (a) minimum, (b) medium, and (c) maximum. $H/d = 3$ has shown better heat transfer performance for all the cross-flow schemes compared with the other configurations.

Culun et al.²⁹ studied the effect of different design parameters on a multijet impinging synergistic heat transfer. The geometry of the jet holes, their arrangement, their density in spanwise and streamwise directions, and the kind of confinement all affect the impingement characteristics. Graphs were drawn for a geometric model (shown in Figure 11) of square and circular jets of 15 in number, arranged in a 3×5 matrix. The arrangement consists of the orifice plate, target plates, and side plates. The effect of jet-to-plate distance (Z_n/d) was shown in Figure 12 for different geometry of the jet holes

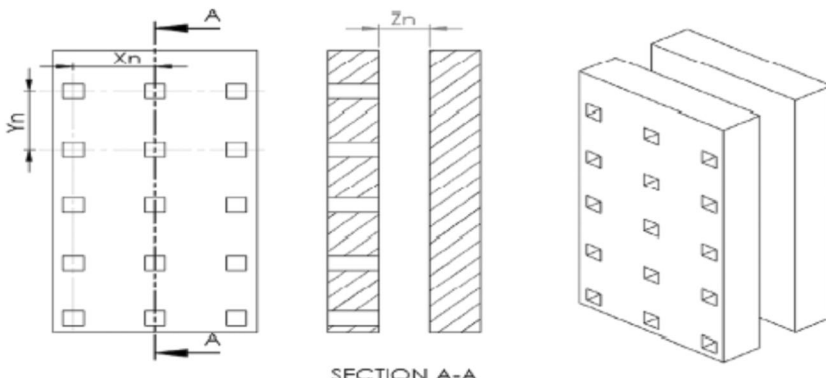


FIGURE 11 Geometric model of square jets²⁹

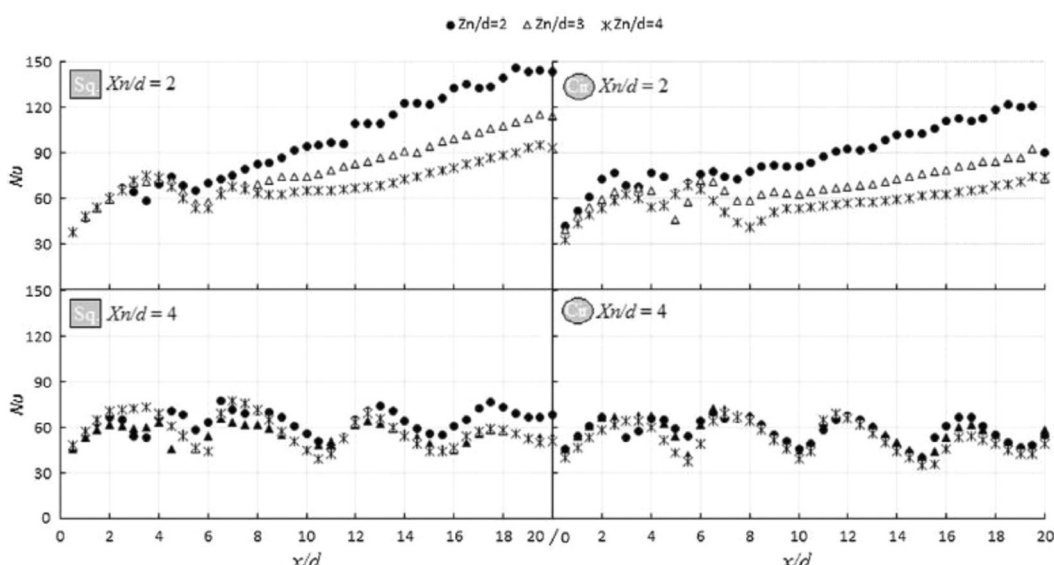


FIGURE 12 Effect of jet-to-plate distance on Nu number²⁹

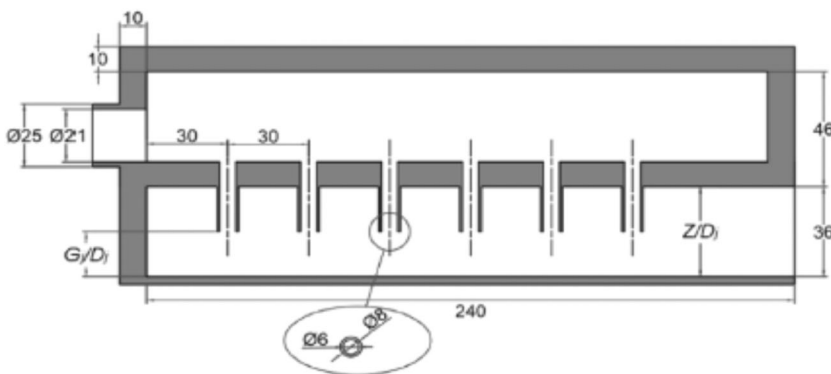


FIGURE 13 Typical test section (all dimensions are in mm)³⁰

(square and circular) at the additional streamwise jet-to-jet pitch distance (X_n/d). The jet behaves like a single jet at low X_n/d values, so the Nu number steadily increases streamwise. This is due to adjacent solid interference. The stagnation points were observed clearly at the high jet-to-plate distance. The Nu number was higher for square jets than the circular jets.

To avoid the effect of cross-flow on heat transfer enhancement in jet impingement cooling, which reduces the effectiveness of jet impingement cooling, Tepe et al.³⁰ investigated the jet impingement cooling with extended jet holes towards the target surface using both experimental and numerical methods. A typical geometry configuration is shown in Figure 13. According to work, heat transfer enhancement was affected by the cross-flow of the fluid between the jet holes and the target surface. A higher gap affects the jet by cross-flow, and the jet bends towards the cross-flow direction, dislocation of jet impingement occurs and reduces heat transfer. So the extension of the jet holes is made by varying the space between the exit of the nozzle and the target surface. G/D_j is the ratio of the gap between the extended hole and the diameter of the jet. Experiments were done for different G/D_j values ranging from 1 to 5 and $G/D_j = 6$ gives the highest spacing nothing but an orifice plate. Extending the nozzle jet with the spacing of $G/D_j = 2$ showed better performance in terms of Nusselt number (both average and local). Figure 14 shows the Nu distribution for Re number 32,500 at different G/D_j ratios. The cross-flow effect is also reduced as the fluid velocity increases with the reducing gap (G/D_j). But reducing the gap increased the pressure drop, which caused an increment in compressor work. So the Performance Evaluation Criterion (PEC) ratio was investigated to check the feasibility of $G/D_j = 2$ spacing and concluded that the most suitable G/D_j spacing is 2.

The summary of literature including the method of investigation and techniques used both experimental and numerical are tabulated in Table 2.

2.3 | Flow and heat transfer studies of impingement and effusion cooling on flat surfaces

Combined Impingement effusion cooling has gained significance due to the high heat transfer coefficients of impingement cooling and high internal convective heat transfer areas by the multiple effusion holes. This concept is generally applied to the gas turbine combustor walls or

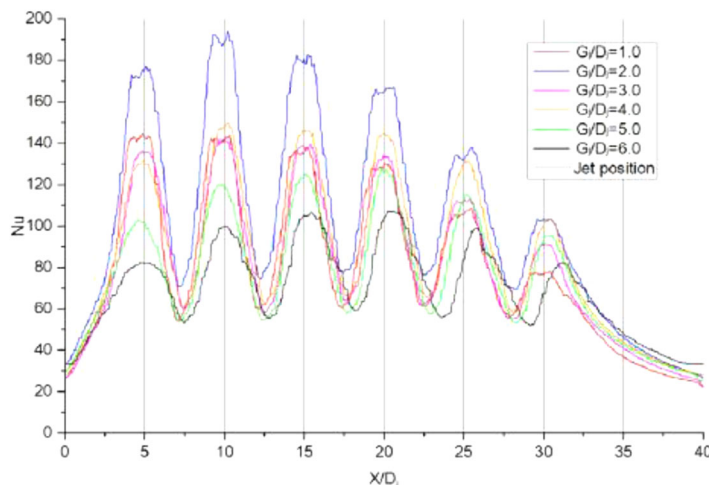


FIGURE 14 Experimental Nu distributions on the target surface for Re 32,500³⁰ [Color figure can be viewed at wileyonlinelibrary.com]

liners, which perform better than film effusion cooling. Figure 15 shows an impingement plate with multiple impingement holes and below that target plate which acts as an effusion plate with multiple effusion holes. Generally, the impingement wall takes the mechanical load while the effusion wall bears the thermal load.³¹

Hollworth and Dagan³² reported average convective heat transfer from a plate perforated to extract the spent air from the impinging jet. The inline arrays showed 35% lower heat transfer rates than the staggered arrangement. This behavior dominates at the lower jet-to-target plate spacing because a significant part of each jet flows directly through the opposing vent without impinging upon the target surface.

Huber and Viskanta³³ reported a study of confined isothermal impinging jets to understand the uniformity of local heat transfer coefficients and average heat transfer coefficients. After impingement, the spent air is removed through the holes on the top confinement wall. They noticed that adding spent air at the exit enhanced the heat transfer, and jet-to-jet spacing affected the convective coefficient. They also pointed out that for a particular target plate distance to jet diameter ratio ($H/d = 6$), adjacent jet interference before impingement causes considerable degradation of convection coefficient compared with single jets. But at low H/d (~1), the interference reduces, and secondary maxima enhance the average convective coefficient. They recommended a spacing of four to obtain a high average Nusselt number and its uniform distribution over the impingement surface.

Viskanta and Huber³⁴ determined that the most significant Nusselt number occurs at the stagnation point when the jet-plate spacing is about equal to the potential core length. They noted that as the spacing falls to one diameter, the highest Nusselt number no longer occurs at the stagnation point but at two downstream peaks (primary and secondary) at approximately one-half and one-and-a-half diameters. These secondary peaks in the Nusselt number profile are related to turbulence caused by the shear layer around the jet's diameter. Additionally, the inner peak is created by the acceleration in the stagnation area, the transition to turbulent flow causes the outer peak, and the secondary peak is caused by the turbulence intensity peak.

TABLE 2 Summary of literature on multiple jet impinging on flat surface

Authors and year	Geometry	Parameters considered	Method of investigation	Technique used	Remarks
Florschuetz et al. (1984) ¹²	Flat surface with multiple jet impingement	Streamwise (X_n/d) and spanwise (Z_n/d); (5, 4), (5, 8), and (10, 4); Mean jet Re : 1000; Jet-to-plate spacing: 1–3	Experimental		The addition of initial cross-flow reduced the mean values of the Nusselt number
Van Treuren et al. (1994) ¹⁴	Flat surface with multiple jet impingement	Streamwise and spanwise hole spacing: 8d; Mean jet Re : 3724–34,368; Jet-to-plate spacing 1	Experimental	Thermochromic liquid crystal technique	The peak Nusselt number is at the hole centerline when the cross-flow is small. As the cross-flow develops, the peak positions are displaced downstream direction
Brizzi et al. (2000) ¹⁵	Flat surface with multiple jet impingement with and without cross-flow	Streamwise and spanwise hole spacing: 4d; Mean jet Re : 12,600; Jet-to-plate spacing: 2	Experimental	Laser Doppler Anemometry	Reported the cellular aspects of flow near the impingement wall and the detachment and reattachment lines in frontier zones between different cells
Hwang and Cheng ¹⁶	Triangular duct with three different outflow orientations: (a) coincident with entry flow, (b) opposed to the entry flow, and (c) both sides open	spanwise hole spacing: 5d; Mean jet Re : 12,600–42,000; Jet-to-plate spacing: 2	Experimental	Transient liquid crystal technique	The outflow orientation significantly affects the local heat transfer characteristics. Among the three tested configurations, they found that the triangular duct with two openings is recommended since it has high wall average heat transfer

(Continues)

TABLE 2 (Continued)

Authors and year	Geometry	Parameters considered	Method of Investigation	Technique used	Remarks
Ekkad et al. (2000) ¹⁷	Two-pass coolant channel with cross-flow induced swirl with three different lateral hole configurations	Spanwise hole spacing: 5d; Mean jet Re : 10,000, 25,000, and 50,000	Experimental	Transient liquid crystal technique	The coolant supply inside the blade from one channel to another appears more promising than the conventional U-bend serpentine channel design
Son et al. (2001) ¹⁸	Flat surface with a staggered arrangement of multiple jet impingement	Streamwise (x/d) and spanwise (z/d) hole spacing: 3–4.8 and 3.75–6; Mean jet Re : 19,552–29,440; Jet-to-plate spacing 1.875–3	Experimental	Transient liquid crystal technique	At the beginning of the impingement plate, the shape of heat transfer distribution under each jet was circular, and near the plate's exit, these shapes were larger and distorted due to the high cross-flow effect
Aldabagh and Sezai (2002) ¹⁹	Flat surface with multiple impingement square jets	Jet-to-jet spacing: 4d, 5d, and 6d; Jet-to-plate spacing: 0.25d and 9d	Computational	ULTRA SHARP flux limiting strategy Bi-CGSTAB iterative method	Heat transfer is strongly affected by jet-to-plate Spacing reported complex flow field with formations of peripheral vortex around each jet and an upwash-fountain flow at the collision point of the jets.
Yan et al. (2004) ²¹	Flat plate with elliptic jets impingement with three different exit flow configurations	Aspect ratio of holes: 4, 2, 1, 0.25, and 0.5; Jet Reynolds number: 1500, 3000, and 4500	Experimental	Transient liquid crystal technique	The two-way exit flow condition is most beneficial to the heat transfer characteristics of an

TABLE 2 (Continued)

Authors and year	Geometry	Parameters considered	Method of Investigation	Technique used	Remarks
Geers et al. (2004) ²²	Hexagonal array of circular jets generally impinging to a flat plate	Jet Reynolds number: 23,000; Jet-to-jet spacing: $2d$; Jet-to-plate spacing: $4d$	Experimental	Particle Image Velocimeter	Their measurement shows the self-induced cross-flow and the wall jets resulted in the formation of a system of horseshoe-type vortices that circumscribe the outer jets of the array
Chambers et al. (2005) ²³	Low aspect ratio impingement channel having 19 holes	Jet Reynolds number: 20,000; Jet-to-jet spacing streamwise: $4.36d$; Jet-to-plate spacing: $1.54d$	Experimental	Liquid crystal technique	The cross-flow strongly influences the heat transfer behavior. They reported that 10% initial cross-flow reduced mean target plate effectiveness by 57%
Dano et al. (2005) ²⁴	Flat surface with confined multiple jet impingement with two different nozzle geometry: (i) circular and (ii) cusped ellipse	Two different thermal boundary conditions: (i) constant heat flux and (ii) isothermal. Jet-to-plate spacing: $(2\text{--}4)d$; Jet Reynolds number: 8500–15,900	Experimental	Digital particle image velocimeter, liquid crystal sheet, and CCD camera	They reported higher heat transfer for circular jet For isothermal case and cusped elliptical geometry for uniform heat flux case
Goodro et al. (2007) ²⁵	Flat surface with multiple impingements	Jet-to-jet spacing: $8d$	Experimental	Custommade HK5184R26 thermofoil heaters, Infrared camera	Presented a correlation equation for spatially averaged Nusselt number

(Continues)

TABLE 2 (Continued)

Authors and year	Geometry	Parameters considered	Method of Investigation	Technique used	Remarks
Xing et al. (2010) ²⁶	Flat surface with an inline and staggered arrangement of multiple jet impingement	Jet Reynolds number: 5200–59,900; Jet Mach number 0.16–0.74 Jet-to-jet spacing: $5d$; Jet Reynolds number: 15,000, 25,000, and 35,000; Jet-to-plate spacing: $3d$, $4d$, and $5d$	Experimental and numerical	Thermochromic liquid crystal technique, and shear stress transport (SST) turbulence model	In the downstream region, the inline pattern was better than the staggered one because, for the inline pattern, the jets were protected from the oncoming cross-flow by the upstream jets. On the other hand, the cross-flow influenced the jets more directly for the staggered pattern
Chambers et al. (2010) ²⁷	Shaped elliptical elongated circular impingement holes	Jet Reynolds number: 20,000; Jet-to-jet spacing Streamwise: $4.36d$; Jet-to-plate spacing: $1.54d$	Experimental and computational	Thermochromic liquid crystal technique, $\kappa-\varepsilon$ turbulence model	The use of shaped holes led to a 16% increase in Nusselt number on the impingement target surface in the downstream half of the cooling passage, along with a reduction of stress concentration factor
Xing and Weighard (2013) ²⁸	Inline multijet impingement on a flat plate for three different cross-flow schemes,	Jet-to-jet spacing: $5d$; Jet Reynolds number: 15,000–35,000; Jet-to-plate spacing: $1d$ – $5d$	Experimental	Transient liquid crystal technique	Reported higher cross-flow at the higher spacing between the target plate and impingement plate

TABLE 2 (Continued)

Authors and year	Geometry	Parameters considered	Method of Investigation	Technique used	Remarks
Culun et al. (2018) ²⁹	Staggered and inclined multijet impingement on the flat plate of circular and square jets	Jet-to-jet space: 2, 3, 4 (spanwise) and 9, 6, 5 (streamwise); Jet-to-plate distance: 2, 3, 4 Re: 15,000	Computational	SST turbulence model	The stagnation points were observed clearly at the high jet-to-plate distance. The Nu number was higher for square jets than the circular jets
Tepe et al. (2020) ³⁰	jet impingement with extended jet holes towards the target surface	Nozzle-to-target plate gap ratio (G/D) = 1, 2, 3, 4, and 5; Jet-to-jet ratio = 5; Jet-to-target plate ratio = 6; Re number = 16,250–32,500	Experimental and Computational	Thermochromic Liquid Crystal technique, SST κ $-\omega$ with low Re correction turbulence model	cross-flow effect reduced with reducing the gap, and Nu number showed better performance at less. But pressure drop increased

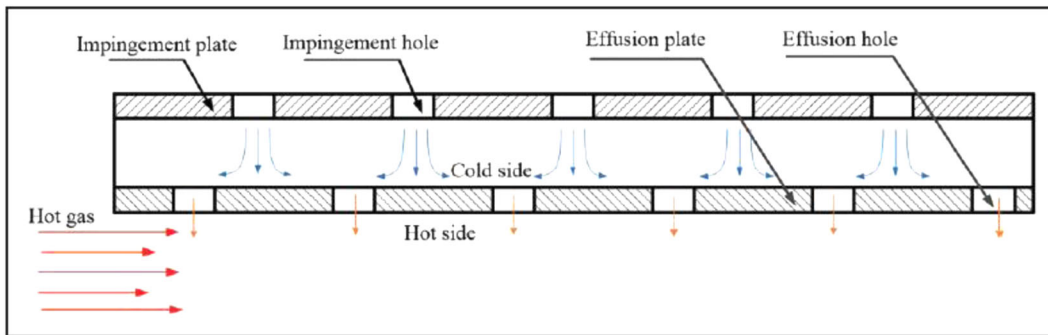


FIGURE 15 Schematic of impingement effusion cooling³¹ [Color figure can be viewed at wileyonlinelibrary.com]

Cho and Rhee³⁵ demonstrated that an impingement/effusion cooling system performs better at the stagnation zone and the center of two impinging jets. This was because secondary vortices were formed, and the flow is accelerated to the effusion holes. Additionally, they observed increased heat/mass transfer as the jet-to-plate gap decreased.

Rhee et al.³⁶ observed significant variation in the heat/mass transfer characteristics of impingement/effusion cooling systems with and without initial cross-flow. The cross-flow disrupts the jet flows ejected from the injection plate and thus weakens the connection between nearby wall jets. Additionally, they reported that as the blowing ratio increases, the heat/mass transfer rates on the effusion/target plate fall, and that at low blowing rates, cooling performance is comparable to that achieved without the initial cross-flow.

Cho et al.³⁷ demonstrated that heat transfer increase was accomplished through jet impingement, flow acceleration into the effusion hole, and interaction of wall jets in the halfway zones for a staggered configuration. The midway region's peak values were even more significant than the stagnation areas, resulting in a considerable rise in the overall transfer rate.

Hong et al.³⁸ conducted an experimental investigation into the impact of impinging jets under the rotating condition on two cooling schemes: array impingement jet cooling and impingement/effusion cooling. They experimented with a constant jet Reynolds number of 5000 for two different H/d configurations (2.0 and 6.0). They reported a significant decrease in heat/mass transfer for $H/d = 6.0$ design due to strong deflection at the leading orientation. However, for lower H/d (2), the reduction of heat/mass transfer due to rotation disappeared.

Chang and Liou³⁹ studied heat transfer on enhanced surfaces with concave and convex dimples. This study reported the impact of Reynolds number variation and H/d variation. Their results show a decrease in the area-averaged Nusselt number with the reduction of the Reynolds number. They developed six correlations for two effused surfaces with concave and convex dimples, to be used in various engineering applications.

Onstad et al.⁴⁰ evaluated the flow and heat transfer characteristics of a staggering array of impingement jets with a diameter of 8.46 mm and an interjet spacing of $2.34d$, where expended fluid was removed by one of six 7.36 mm diameter extraction holes positioned regularly around each jet. The jet impingement apparatus is shown in Figure 16. They altered the jet Reynolds numbers (2600 and 5300) and visualized the three-dimensional flow fields inside the cooling cavity using magnetic resonance velocimetry. Their findings demonstrate a seamless velocity shift from an impingement jet to the extraction hole without significant vertical structures.

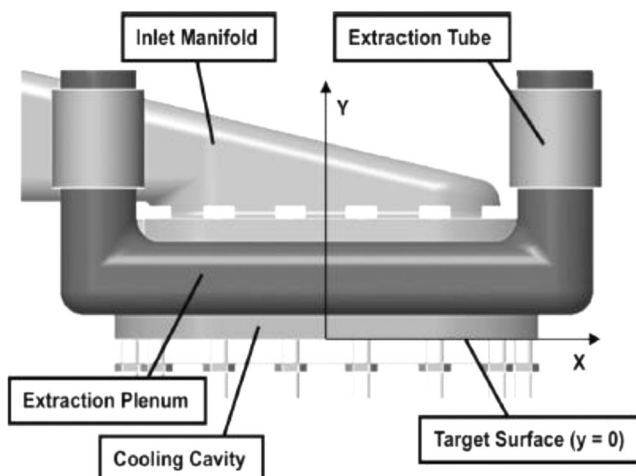


FIGURE 16 Jet impingement apparatus⁴⁰

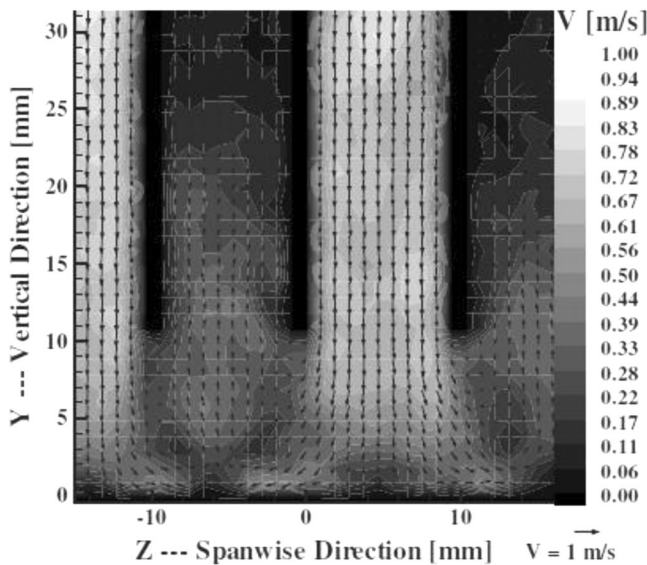


FIGURE 17 Velocity magnitude contours (in a plane) and velocity vectors zoomed in to show the flow structure inside the cooling cavity (jet is impinging from the top)⁴⁰

However, the internal cross-flow established asymmetric counterrotating vortices upstream and downstream, relative to the cross-flow direction of each impingement jet. The small interjet spacing of the impingement array enabled a large Nusselt number due to an increase in the area encompassed by primary stagnation heat transfer. They suggested that improving heat transfer rates was possible by eliminating the cooling cavity cross-flow. Figure 17 shows the typical velocity magnitude contours and flow structure using the magnetic resonance velocimetry for a cooling cavity.

TABLE 3 Averaged Nu number for different Re at an aspect ratio of 0.5 (elliptical jet hole) for a jet-to-plate spacing 3⁴¹

Re	Type		
	Side	Middle	Staggered
2000	12.186	11.942	10.700
3000	18.523	21.832	18.311
4000	23.603	23.293	25.175

Chiu et al.⁴¹ observed that decreasing the jet-to-plate separation enhances impinging force and cross-flow. However, the impinging force increase is more significant than the cross-flow increment. This increases overall heat transfer. Among the three possible configurations for a film hole on the target plates, named side, middle and staggered types, the enhancement on the middle-type target plate was more significant than the other types. The details are shown in Table 3.

Hoberg et al.⁴² reported a Nusselt versus Reynolds correlation for a jet-to-target spacing of one jet diameter. They considered a jet plate where six local effusion holes surround each jet. Their results indicate smaller-scale arrays gave higher dimensional heat transfer coefficient as the heat transfer coefficient varied with the -0.41 power of the diameter for fixed jet velocity and jet-to-target spacing.

Kim et al.⁴³ investigated the effect of pin spacing (ratio of pin spacing to diameter, sp/d) on heat/mass transfer characteristics for a multilayered impingement effusion cooling system with pins. Heat transfer characteristics on the effusion plate for higher sp/d ($sp/d = 6$) are similar to the little impingement jet cooling without pins. Increasing the number of pins ($sp/d = 1.5$ and 2) enhanced the heat transfer in front of the pins and at the effusion holes on both the plates due to the complex vortex pattern. They also concluded that the improved heat transfer performance compensates for the increased pumping power due to more pins.

The summary of literature including method of investigation and techniques used in both experimental and numerical are tabulated as shown in Table 4.

2.4 | Flow and heat transfer study of combined impingement-film cooling on flat surfaces

Ekkad et al.⁴⁴ mentioned that film extraction reduces the cross-flow effect and increases jet impingement heat transfer. As the flow migrates towards the effusion holes at a higher velocity than the cross-flow, the Nusselt number increases between the jets. Further, they noticed that the heat transfer distribution on the target surface varies with the exit flow orientation.

Miao and Wu⁴⁵ pointed out that “no literature so far has systematically investigated both the internal impingement cooling and external film cooling together with a numerical approach,” focused on investigating the effects of the shape of the hole and blowing ratio for a combined impingement and film-cooling configuration. By comparing with isolated film cooling, they found that, due to impingement, a less degree of jetting flow occurred in the coolant tube, leading to higher effectiveness. Though they analyzed film-cooling flow extensively, impingement flow and heat transfer behavior on the internal surface is not reported.

TABLE 4 Summary of literature on a flat surface with impingement and effusion cooling

Authors and year	Geometry	Parameters considered	Method of investigation	Technique used	Remarks
Hollworth and Dagan (1980) ³²	Flat plate with effusion holes with the staggered and inline arrangement of jets	Jet orifice diameter: 5.0 and 2.5 mm; Jet Reynolds number: Re 3000–35,000; Nondimensional jet-to-jet spacing: 5, 10, 15, and 20	Experimental	Liquid crystal coatings	The inline arrays showed much lower (~35%) heat transfer rates compared with the staggered arrangement, and this behavior is more pronounced at the lower jet-to-target plate distance
Huber and Viskanta (1994) ³³	Heated flat surface with 3 × 3 array of impinging jets with effusion holes	Jet-to-jet spacing: $6d$; Jet Reynolds number: 3500–20,400; Jet-to-plate spacing: 0.25 d , 1 d , and 6 d	Experimental	Bandpass filters, electronic digitizer	The addition of spent air at the exit enhances the heat transfer rate, and Jet-to-jet spacing affects the convective coefficient
Cho and Rhee (2001) ³⁵	Flat plate with impingement and effusion holes	Jet-to-jet spacing: $6d$; Jet Reynolds number: 5000–12,000; Jet-to-plate spacing: 0.33 d –10 d	Experimental	Naphthalene sublimation method	Reported the formation of secondary vortices and flow acceleration to the effusion holes leads to higher heat transfer at the stagnation region and the center of two impinging jets
Rhee et al. (2003) ³⁶	Flat plate with impingement/effusion holes with cross-flow effects	Jet-to-jet spacing: $6d$; Jet Reynolds number: 10,000; Jet-to-plate spacing: $2d$	Experimental	Naphthalene sublimation method	Reported that as the blowing ratio increases, the heat/mass transfer rates on the effusion/target plate decrease, and for the low blowing rate, the cooling performance is similar to that without the initial cross-flow

(Continues)

TABLE 4 (Continued)

Authors and year	Geometry	Parameters considered	Method of investigation	Technique used	Remarks
Cho et al. (2008) ³⁷	Flat plate with impingement/effusion holes with a small hole spacing	Jet-to-jet spacing: $3d$; Jet Reynolds number: 3000–14,000; Jet-to-plate spacing: $1d$ – $3d$	Experimental and computational	Naphthalene-coated test plate; renormalization group κ - ϵ turbulence model with enhanced wall treatment	Pointed out that for the staggered arrangement, heat transfer enhancement was achieved by jet impingement, flow acceleration into effusion holes, and interaction of wall jets in the midway regions
Hong et al. (2009) ³⁸	Rotating jet impingement on flat plate with impingement and effusion holes	Jet-to-jet spacing: $6d$; Jet Reynolds number: 5000; Jet-to-plate spacing: $2d$ – $6d$	Experimental	Naphthalene-coated test plate	At higher jet-to-plate spacing, the jet was strongly deflected at the leading orientation, resulting in a significant decrease in heat/mass transfer
Onstad et al. (2009) ⁴⁰	Flat plate with impingement/effusion holes	Jet-to-jet spacing: $2.34d$; Jet Reynolds number: 2000–10,000; Jet-to-plate spacing: $1.18d$	Experimental	Magnetic resonance velocimeter	The internal cross-flow established asymmetric counterrotating vortices upstream and downstream, relative to the cross-flow direction of each impingement jet. The small inter jet spacing of the impingement array enabled a large Nusselt number
Chiu et al. (2009) ⁴¹	Elliptic jet impingement on film-cooled flat	Jet-to-jet spacing: $3d$	Experimental	Liquid crystal thermography, digital color camcorder	Lowering jet-to-plate spacing both impinging force and

TABLE 4 (Continued)

Authors and year	Geometry	Parameters considered	Method of investigation	Technique used	Remarks
Hobeng et al. (2010) ⁴²	Flat plate jet impingement with local extraction	Jet-to-jet spacing: 2.34d; Jet Reynolds number: 2000–4000; Jet-to-plate spacing: 1.5d–4.5d	Experimental 500–10,000; Jet-to-plate spacing: 0.44d–3.97d	Stereolithography (SLA) and computer numerical control drilling	Increasing jet-to-target spacing was found to decrease average heat transfer in all cases
Kim et al. (2017) ⁴³	Flat plate with impingement and effusion cooling along with pins	Pin spacing to diameter ratio ($sp/d = 1.5, 2$ and 6), height to diameter = 0.25; Re based on the hole diameter = 3000	Experimental and computational	Naphthalene sublimation method and shear stress transport γ model	The increasing no of pins increased the heat transfer and pumping power

Oh et al.⁴⁶ conducted experiments on a stainless steel flat plate for the combined impingement and film-cooling configurations. They reported that the effectiveness would increase with the blowing ratio due to the enhancement in both impingement and film cooling. Further, they examined the effect of the jet-to-plate spacing but did not find more than a 3% change in the film-cooling effectiveness. They attributed this small change to the film hole's high length to diameter ratio.

Jingzhou et al.⁴⁷ mentioned that decreasing the center-to-center spacing of adjacent holes and enhancing the blowing ratio could increase average cooling effectiveness. The inclusion of impingement resulted in the notable rise of the heat transfer in the effusion plate, attributed to the strong attraction of secondary flow by effusion holes. The difference between surface temperature and fluid temperature was reduced along the streamwise direction. The total heat flux was more extensive on the mainstream surface than on the coolant side of the effusion plate.

Jung et al.⁴⁸ used a polycarbonate plate to study the impingement and film-cooling configuration. The arrangement for the graph shown in Figure 18 was a staggered arrangement with film-cooling holes inclined at 35° along with the straight impinging holes. These results were compared with the previously done inline arrangement study for different streamwise distances along the span of the flat plate. They found that the effectiveness values obtained

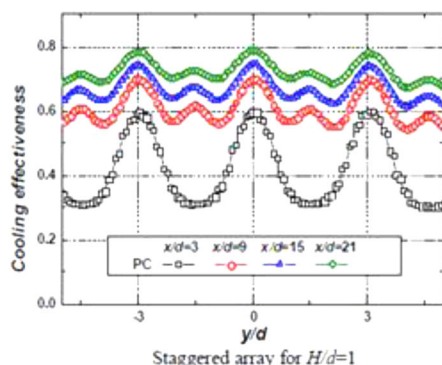
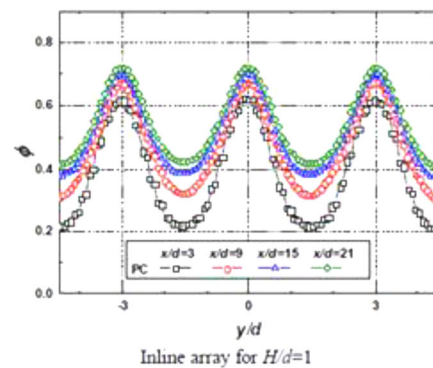
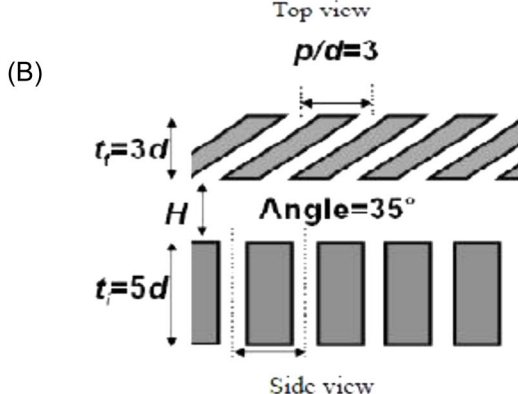
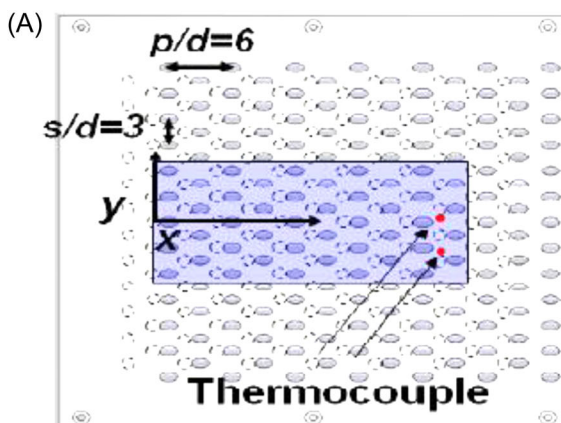


FIGURE 18 Schematic view of hole arrangement for staggered array (left) and local plots of cooling effectiveness for $M = 0.3$ (right)⁴⁸ [Color figure can be viewed at wileyonlinelibrary.com]

from the staggered arrangement were more uniform than the inline. As the jet-to-plate spacing changes, significant changes in the heat transfer coefficient of the impingement jet are observed. However, little difference is noticed in the external effectiveness.

Ghorab⁴⁹ computed the cooling performance for hybrid and louver schemes for the different blowing ratios. Their film-cooling configuration is designed to reduce the lift-off. They reported that with an increase in blowing ratio, the hybrid and the louver schemes give higher film-cooling effectiveness. However, they did not consider the conjugate heat transfer effect and pointed out the need to carry out the study over an airfoil with including the conjugate effect.

Mensch and Thole⁵⁰ studied the overall performance of three cooling strategies on the end wall of a seven-blade cascade: only impingement cooling, alone film cooling, and a combination of film and impingement cooling. They discovered that the combined film and impingement cooling case was the most successful of the three. It can be seen in Figure 19 for the blowing ratio ($M_{\text{avg}} = 1$) and at normalized chord length ($x/C_{\text{ax}} = 0.22$). They also reported, with film cooling alone, that higher cooling effectiveness in the vicinity of the hole exit did not improve considerably elsewhere in the passage. Similarly, for impingement cooling alone, the effectiveness distribution was uniform and demonstrated a clear improvement as coolant flow rates increased.

Kosarev et al.⁵¹ monitored pressure in a radial jet with and without whirling the input flow in the prechamber using a Pitot tube. They discovered that when deposition occurs at less than 4–6 gauges from the nozzle exit, the solid particle velocity and temperature are nearly homogeneous over the jet cross-section.

Yang et al.⁵² investigated the effect of impingement on the adiabatic film-cooling effectiveness for the case with dimples on the target surface in which film coolant enters post impingement of the spherical dimples onto the film surface. The physical model of the configuration with dimples is shown in Figure 20. According to the study, at moderate and high blowing ratios, the jet-to-plate distance has a prominent effect on the film-cooling effectiveness. At $M = 1$, the $H/d = 2$ has shown better performance than the case without dimples. For other cases ($H/d = 1, 4$, and 6) the performance is lower than that of the base configuration at $M = 1.5$. Results of adiabatic film-cooling effectiveness were compared with the conjugate

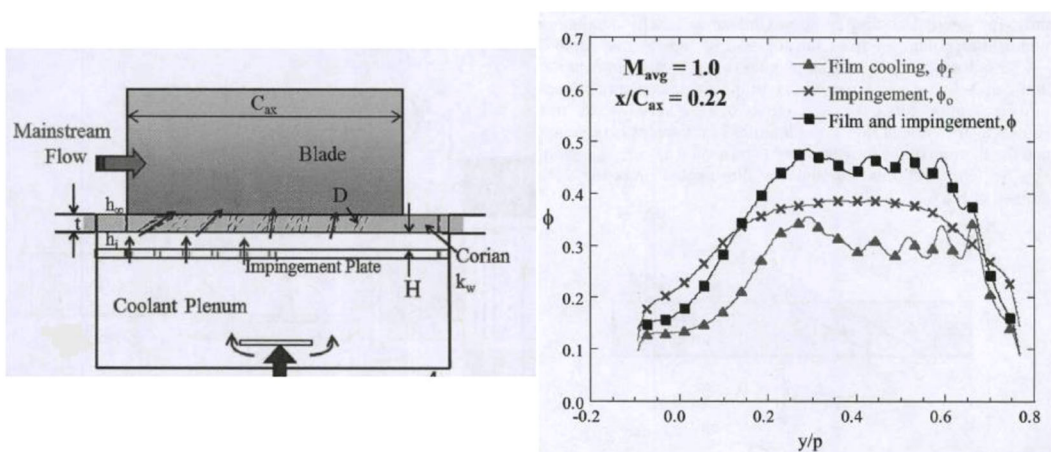


FIGURE 19 Blade configuration for the study (left), overall film-cooling effectiveness for all configurations at blowing ratio ($M_{\text{avg}} = 1$), and normalized chord length ($x/C_{\text{ax}} = 0.22$) along normalized pitch (right)⁵⁰

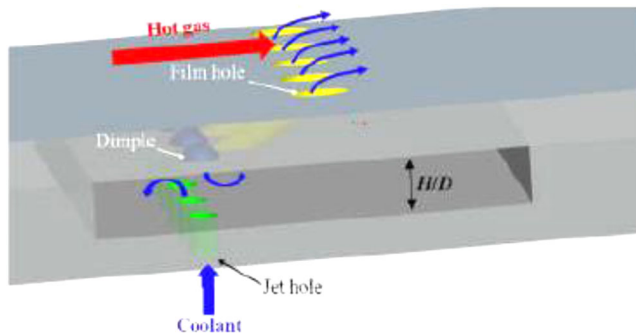


FIGURE 20 Physical model of the configuration⁵² [Color figure can be viewed at wileyonlinelibrary.com]

studies and overestimations were observed when conjugate studies were neglected. This has shown the importance of the conjugate effect as it can be compared with the performance of realistic gas turbine engines.

The summary of literature including the method of investigation and techniques used both experimental and numerical are tabulated as shown in Table 5.

2.5 | Investigations of conjugate heat transfer on a flat plate

In the heat transfer studies described in the preceding literature, the conjugate studies, even on isolated impingement or film cooling, are limited. Many previous researchers used constant temperature or heat flux on the target surface as thermal boundary conditions, ignoring the heat conduction within the plate. However, for a combined impingement and film cooling, the problem is inherently a conjugate one as the boundary condition on the vane and blade surface cannot be imposed for a realistic case. Additionally, as demonstrated by Luikov,⁵³ and Prasad and Sarkar,⁵⁴ thermal conductivity and thickness ratios determine the significance of the conjugate study. Few studies where the conjugate effects are studied on a flat plate are mentioned below.

Sweeney and Rhodes⁵⁵ developed the matched Biot number (Bi) model for conjugate heat transfer analysis. They employed a flat plate made of a lower thermal conductivity material chosen to match the Biot number to the engine's operating conditions. The matching Biot number assures that the ratio of convective heat transfer at solid surfaces to conduction through solids corresponds to the engine's operating conditions. To match the thermal conductivity of Bi in the flat plate model to that of an engine, the model was made using the material with approximately three times the thermal conductivity of engine material. This was because the heat transfer coefficients to the engine had been lowered by a factor of around three in a big-scale plant.

Yang and Tsai⁵⁶ employed a low Reynolds-turbulence model to predict the heat transfer coefficient for the flat plate model to examine conjugate heat transfer. They anticipated impingement surface temperature change by imposing varied uniform heat flow values at the bottom surface.

Panda and Prasad⁵⁷ studied the conjugate effect by considering a flat plate with impingement and film cooling combined. They used three different conductivity materials (Materials A, B, and C) exposed to three different blowing ratios and found that the heat peak is

TABLE 5 Summary of literature on flat plate with impingement and film cooling

Authors and year	Geometry	Parameters considered	Method of investigation	Technique used	Remarks
Ekkad et al. (1999) ⁴⁴	Flat plate with impingement and film-cooling holes	Jet-to-jet spacing: $4d$; Jet Reynolds number: 400–20,000; Jet-to-plate spacing: $3d$	Experimental	Transient liquid crystal technique	Reported increase in Nusselt number as the flow migrates towards the effusion holes at higher velocity. Further, they noticed that the heat transfer distribution on the target surface varies with the exit flow orientation
Miao and Wu (2006) ⁴⁵	Flat plate with impingement and different-shaped film-cooling holes	Jet-to-jet spacing: $2d$; Jet-to-plate spacing: $2d$; Blowing ratio: 0.3–1.5	Computational	Low Reynolds' number $\kappa-\varepsilon$ turbulence model	They found that, due to impingement, less jetting flow occurred in the coolant tube, leading to higher effectiveness compared with isolated film cooling
Oh et al. (2008) ⁴⁶	Flat plate with impingement and film-cooling holes	Jet Reynolds number: 3000–5000; Jet-to-jet spacing: $3d$; Jet-to-plate spacing: $1d$; Blowing ratio: 0.3–0.5	Experimental	Infrared thermal camera	Reported that the effectiveness would increase with blowing ratio due to the enhancement in both impingement and film cooling. Further, they examined the effect of jet-to-plate spacing but did not find more than 3% change in the film-cooling effectiveness. They attributed this small change to high length to diameter ratio of film hole used by them
Jingzhou et al. (2009) ⁴⁷	Flat plate with impingement and film-cooling holes	Jet-to-jet spacing: $(1.5\text{--}2.5)D$; Jet-to-plate spacing: $(3D)$; Blowing ratio: 0.3–1.5	Computational	Standard $\kappa-\varepsilon$ turbulence model	The inclusion of impingement resulted in a notable rise in the heat transfer in the effusion plate, attributed to the strong attraction

(Continues)

TABLE 5 (Continued)

Authors and year	Geometry	Parameters considered	Method of Investigation	Technique used	Remarks
Jung et al. ⁴⁸	Flat plate with impingement and film-cooling holes for both inline and staggered arrangements	Jet-to-jet spacing (streamwise): $3d$; pitchwise: $6d$; Jet-to-plate spacing: $1d$, $3d$, and $5d$; blowing ratio: 0.3–1.5	Experimental	Infrared thermography	As the jet-to-plate spacing changed, they noticed considerable changes in the heat transfer coefficient of the impingement jet. However, little difference is noticed in the external effectiveness of secondary flow by effusion holes
Ghorab (2011) ⁴⁹	Flat surface with hybrid and the louver schemes	Jet Reynolds number: 1.24×10^4 – 3.68×10^4 ; Jet-to-plate spacing: $1d$; Blowing ratio: 0.5–1.5	Experimental	Thermochromic liquid crystal technique	Hybrid and the louver schemes provided a high local and average film-cooling effectiveness. However, they did not consider the conjugate heat transfer effect and pointed out the need to carry out the study over an airfoil with including the conjugate effect
Mensch and Thole (2013) ⁵⁰	Flat surface with only impingement, only film cooling, and combined film and impingement cooling	Jet diameter: 4.4 mm; Blowing ratio: 0.6–2	Experimental	Laminar flow element, infrared thermography	They found the combined film and impingement cooling case to showcase the highest effectiveness of the three cases. The effectiveness distribution was uniform for impingement cooling alone and showed clear improvement with increasing coolant flow rates

TABLE 5 (Continued)

Authors and year	Geometry	Parameters considered	Method of Investigation	Technique used	Remarks
Yang et al. (2016) ⁵²	Impingement on Target plate with dimples and film-cooling holes	Jet-to-plate distance ratio (H/d) = 1, 2, 4, and 6; Eccentricities b/w dimple center and film hole center = 0, 2, and 4; Blowing ratio (M) = 0.5–2 Jet Reynolds' number = 2830–11,330	Computational	Shear stress transport $\kappa-\omega$ turbulence model	At moderate and high blowing ratio jet-to-plate distance shown importance on effectiveness, the conjugate effect gives reliable results compared with the adiabatic

higher in the higher conductivity material. They also found that the effectiveness variations are lower for the higher conducting materials. Figure 21 shows the nondimensional temperature distribution at a vertical plane above the interaction surface for one row of film-cooling holes for three different materials.

Guo et al.⁵⁸ examined the transient heat transfer characteristics of circular air jet impingement on a flat plate both computationally and experimentally. Stainless steel 304 material is used for the target plate. The nondimensional distance between the nozzle exit and the target plate (H/d) is altered between 4 and 8 to obtain the variation in the Nusselt number at $Re = 34,000$. The Nu number at stagnation increased from 144 to 175 when the H/d rose from 4 to 8.5. The uncertainty analysis of 2D axis-symmetric transverse inverse heat transfer models was also presented.

Devaraj and Ganesh⁵⁹ conducted a conjugate heat transfer analysis on a flat plate with jet and impingement cooling. The $\kappa-\omega$ shear stress transport (SST) turbulence model was employed for this computational analysis. The enhancement of the effectiveness is observed with an increase in Reynolds' number (389–2140) which is due to the increase of the local Nusselt number. Flow with Reynolds' number 972, and blowing ratio of 0.6 has shown the best film attachment and enhanced the film effectiveness.

The summary of literature including the method of investigation and techniques used both experimental and numerical are tabulated as shown in Table 6.

3 | FLOW AND HEAT TRANSFER STUDIES OF IMPINGING JETS ON CURVE PLATE

Rigorous literature was reviewed to study the flow and heat transfer behavior on the curve plate. The curve plate approximates the leading edge of a gas turbine vane. Most of the literature had shown the experimental work on the different jet-to-plate spacing (H/d) ratios and at different Reynolds' numbers.

3.1 | Flow and heat transfer studies of multiple impinging jets on curve plate

Chupp et al.⁶⁰ evaluated the heat transfer coefficient for round jets impinging on a concave surface simulating the leading edge of a turbine blade. Their trials included orifices ranging from 0.15 to 6.6 mm, nozzle-to-plate spacings ranging from 0.79 to 3.17 mm, and concave plate diameters ranging from 1 to 2.4 mm. A cold model was developed to measure heat transfer using Joulean dissipation. They created the target surface by sandwiching multiple platinum heater strips together with insulation. The wall temperature distributions were obtained from the platinum strips' electrical resistance measurements. Their findings included correlations for heat transfer along the stagnation line and average heat transfer over the leading-edge section of the target surface.

Metzger et al.⁶¹ investigated the heat transfer between a single line of circular jets and a concave cylindrical surface. The maximum heat transfer coefficient was reported for the nozzle-to-plate distances of the unit jet diameter. Correlations between the average Stanton number and Reynolds number and distance along the target surface were proposed. For comparison, results for two-dimensional jets impinging on a target concave surface were

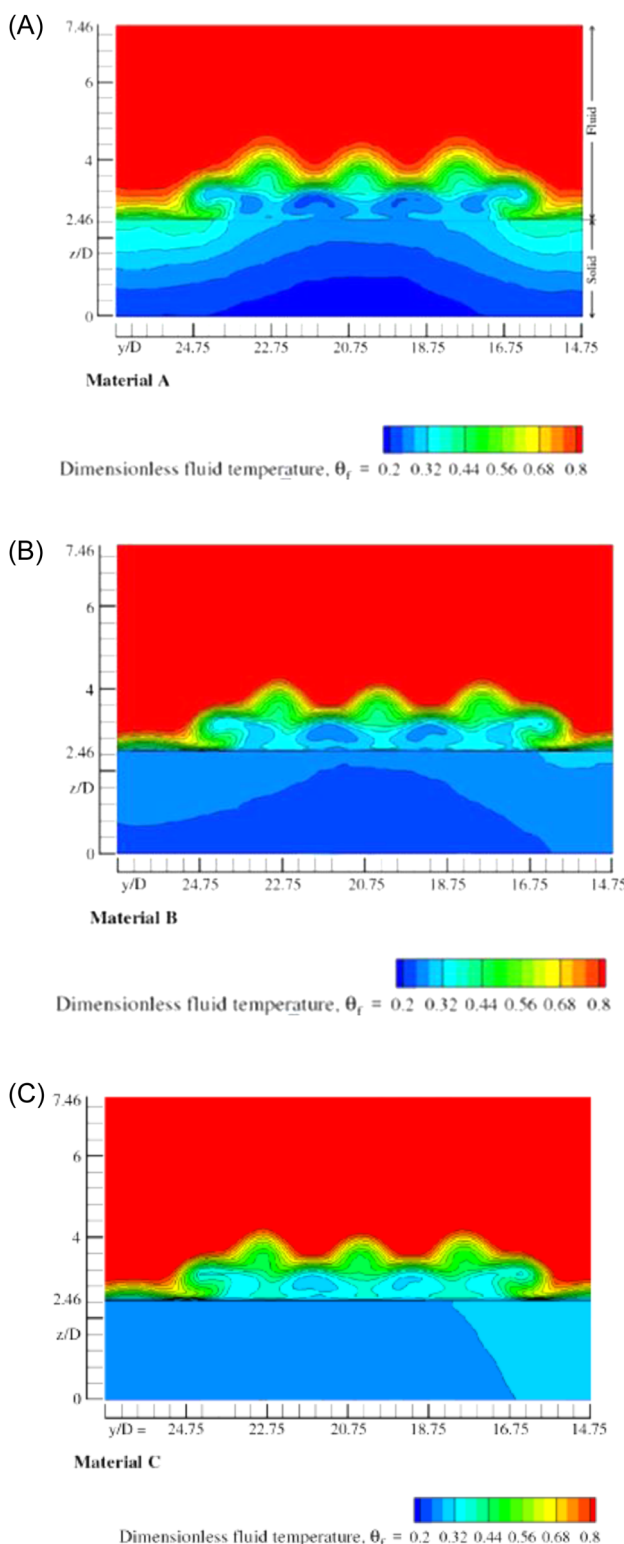


FIGURE 21 Dimensionless temperature distribution along a vertical plane for (A) Material A, (B) Material B, and (C) Material C for blowing ratio ($M = 1^{57}$) [Color figure can be viewed at wileyonlinelibrary.com]

TABLE 6 Summary of literature on conjugate heat transfer study on a flat plate

Authors and year	Geometry	Parameters considered	Method of investigation	Technique used	Remarks
Luikov (1974) ⁵³ and Prasad and Sarkar (1993) ⁵⁴	Laminar flow over a flat plate with conjugate boundary condition	Reynolds number: $10^6 k$; 0.46 W/m K ; 0.68 W/m K ; $P_r: 1.75$ and 0.7	Mathematical and experimental	Boundary layer equation and Brun number	Concluded that thermal conductivity and thickness ratios are critical parameters in conjugate study
Sweeney and Rhodes (2000) ⁵⁵	Flat plate with Lamillloy snowflake design	Blowing ratio: 0.7–1.5; Free stream Reynolds number: 1.0×10^6 – 1.8×10^6 ; The material used is –6 to 4 titanium (conductivity 2.5 times lower than the cast nickel-base superalloys used in turbine airfoil)	Experimental	Infrared imaging system	Proposed the “matched Biot” models by which laboratory experimental results can be used for engine conditions. They used material with thermal conductivity approximately three times less than engine material
Yang and Tsaei (2007) ⁵⁶	Flat plate with turbulent impinging jets	Reynolds number: $16,100$ – $29,600$; Jet plate spacing: $(4\text{--}10)d$	Computational	Low Reynolds' number $\kappa-\omega$ turbulence model; Power law scheme	They predicted impingement surface temperature variation by imposing different uniform heat flux values at the bottom surface
Panda and Prasad (2014) ⁵⁷	Flat plate with combined impingement and film cooling	Jet Reynolds number: 825; Jet-to-jet spacing spanwise: 4.94D, Streamwise: 6.96D; Jet-to-plate spacing: 1.26d; Blowing ratio: 0.6–1.6; Thermal conductivities of 0.2, 1.5, and 15 W/m K	Experimental and computational	Thermochromic liquid crystal technique, shear stress transport (SST) $\kappa-\omega$ turbulence model	Heat peak up is more in the higher conductivity material. They also found that the effectiveness variations are lower for the higher conducting materials

TABLE 6 (Continued)

Authors and year	Geometry	Parameters considered	Method of investigation	Technique used	Remarks
Guo et al. (2017) ⁵⁸	Flat plate with circular air jet impingement	Diameter of nozzle = 6 mm; Jet-to-plate space ratio (H/d) = 4–8.5; Re = 14,000–53,000	Experimental and computational	renormalization group $\kappa-\varepsilon$ turbulence	Nu number increased with an increase in the H/d ratio
Devaraja and Ganesh (2021) ⁵⁹	Jet impingement on a flat plate	Blowing ratio = 0.6–2.6; Re = 389–2140; Jet-to-plate space ratio (H/d) = 1.26	Computational	SST $\kappa-\omega$ turbulence model	Effectiveness increased with an increase in Re number

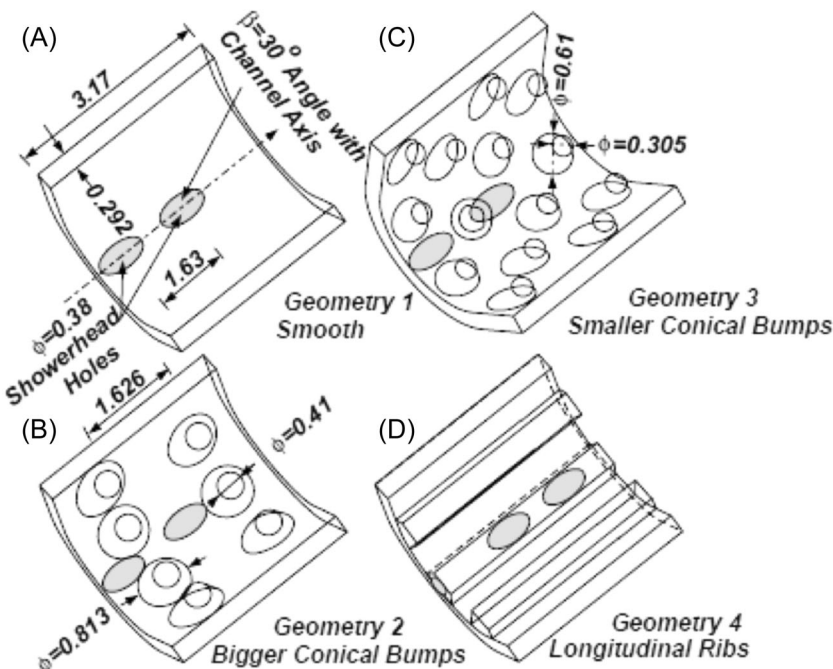


FIGURE 22 Different target surface geometries⁶⁶

reported. They discovered that lines of circular jets impinging on a concave surface generated significantly greater heat transfer rates than identical two-dimensional slot jets.

Tabakoff and Clevenger⁶² published the platenwise local and average heat transfer coefficients on a concave surface for (i) a slot jet, (ii) a single row of round jets, and (iii) an array of round jets. The most significant heat transfer occurred when a single row of smaller-diameter jets with a larger spacing-to-diameter ratio was used. The change in jet position from the center of symmetry to the side results in a modest increase in overall heat transfer. It was also reported that the presence of the solid particle in the impinging air decreases heat transfer by forming an insulation film on the target surface.

Metzger et al.⁶³ investigated the heat transfer properties of impingement into cavities simulating a gas turbine airfoil's cooled leading edge. Their investigation considered two-dimensional slot jets and a single line of uniformly spaced circular jets. For leading-edge semicircular models, correlations for average Stanton numbers as a function of Reynolds number and half-length of target surface were proposed. Higher heat transfer rates for sharp leading edge even at large jet heights were noticed.

Hrycak⁶⁴ determined the stagnation and average heat transfer expressions for a row of impinging jets on a large-scale concave cylindrical surface, simulating the geometric ratio of the leading edge of a turbine blade. The heat transfer expressions for the stagnation point and wall jet zone were calculated using Froessling's solution to the governing equations and the Colburn analogy. Experiments were conducted to compare the values obtained from expressions developed and found good agreement between the two. It was also stated that the flat plate results obtained with single jets could be applied to the row of jets impinging on the semicylindrical surface with certain modifications.

Bunker and Metzger⁶⁵ investigated local heat transfer in a simulated airfoil leading-edge region using impingement cooling on large-scale models of turbine blade leading edges. They conducted the transient studies using the direct application of “melting point coatings” to the test surface and automated data-collecting devices. Impingement air is supplied by a single line of equally spaced multiple jets in the opposite chordwise direction from the leading-edge region. Their investigation altered the jet Reynolds number, airfoil leading-edge sharpness, jet pitch-to-diameter ratio, and jet nozzle-to-apex travel distances. The authors reported the local two-dimensional surface Nusselt number distributions throughout the airfoil surface. They found an increase in overall leading-edge heat transfer when the jet nozzle pitch-to-diameter ratio is decreased from 4.67 to 3.33. They found that close nozzle-to-apex spacing and higher radius ratios were desirable for improved, leading-edge heat transfer.

Taslim et al.⁶⁶ determined the convective heat transfer coefficient for multiple jets impinging on a roughened surface of an airfoil leading edge. Four types of walls were chosen for their study: (i) smooth walls, (ii) walls with high surface roughness, (iii) walls with conical bumps, and (iv) walls with tapering radial ribs. The different target surface geometries are shown in Figure 22. Among the four surfaces evaluated, conical bumps provided the most remarkable heat transfer improvement (about 40%). They reported enhanced heat transfer by roughening the target surface.

Nirmalan et al.⁶⁷ quantified an elliptic airfoil's internal heat transfer coefficient with an impingement insert using infrared thermography and inverse conduction analysis. Their technique accurately anticipated the full-surface internal heat transfer coefficient distributions

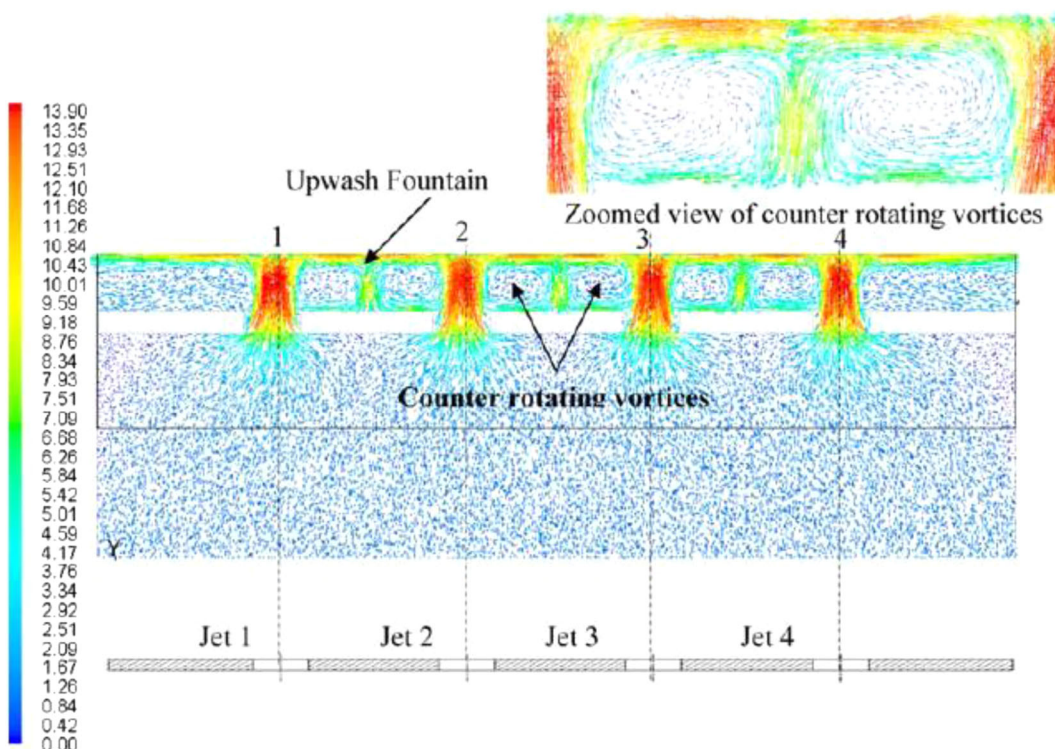


FIGURE 23 Velocity vectors (m/s) on vertical plane of concave target plate geometry for $H/d = 1$, $Re = 6750$, and $c/d = 3.33^{73}$ [Color figure can be viewed at wileyonlinelibrary.com]

for the prototype and production of metallic airfoils in a completely nondestructive and nonintrusive way.

Iacovides et al.⁶⁸ used the liquid crystal technique and LDA to know the heat transfer and flow characteristics of the single row of circular jets impinging on the semicylindrical concave surface with and without rotation. They reported a higher Nusselt number region around the impingement points and a secondary peak between impingement jets. However, the rotational effect reduces the heat transfer and causes the disappearance of the secondary peak.

Fregeau et al.⁶⁹ used Kriging interpolation to derive correlations for the maximum and average Nusselt numbers in a three-dimensional hot air jet array impinging on a curved surface. Computations were carried out for high jet Mach numbers ($M = 0.4, 0.6$, and 0.8), and the Spalart–Allmaras (S-A) turbulence model was used. The influence of Mach number was more predominant than the nozzle–nozzle distance.

Ibrahim et al.⁷⁰ conducted CFD experiments for heat transfer with single and multiple jet impingements over flat, concave, and convex surfaces. They have carried out the parametric variation of (1) jet Reynolds number (3000–23,000) and (2) jet-to-target-plate spacing (2–14) using four CFD models, namely, (1) laminar flow, (2) standard $\kappa-\epsilon$, (3) $\kappa-\omega$, and (4) v^2-f models available in fluent. They concluded that the v^2-f model showed the best overall agreement with the data for single and multiple jets. The $\kappa-\omega$ model shows marginal agreement while the $\kappa-\epsilon$ model over-predicted the Nusselt number.

Fenot et al.⁷¹ investigated heat transfer in the presence of a row of hot circular jets impinging on a semicylindrical concave surface. A thin heat foil method and infrared thermography were used to determine the heat transmission. To investigate the effect of relative curvature between 0.15 and 0.2, jet tubes of various diameters were employed. The result of Reynolds number (10,000, 23,000), interjet spacing (4), and the effect of target plate spacing (2, 5) were also studied. Heat transfer was found to have enhanced near the impingement zone for large values of relative curvature.

Hong et al.⁷² examined the heat/mass transfer characteristics of stationary and rotational impinging jets on a concave surface. They conducted mass transfer experiments using the naphthalene sublimation technique and plotted the Sherwood number distribution. The results were reported for a jet Reynolds number of 5000 with an interjet spacing of three times the diameter of the jet orifice. Compared with the flat surface, the concave surface accelerated heat/mass transfer with increasing spanwise direction due to the curvature effect.

Kumar and Prasad⁷³ used computational fluid dynamics to determine the flow and heat transfer characteristics of a row of circular jets impinging on a concave surface. They varied factors such as the jet Reynolds number (5000–67,800), the distance between the jets to the jet diameter ratio ($c/d = 3.33$ and 4.67), and the distance between the target plate and the jet diameter ratio ($H/d = 1, 3$, and 4). They identified the presence of a pair of counterrotating vortices, an upwash fountain flow, and entrainment using the $\kappa-\omega$ turbulence model with Fluent 6.2.16. They concluded that when $H/d = 1$, larger heat transfer coefficients are produced than when $H/d = 3$ or 4 and that heat transfer is enhanced with a lower c/d value. Figure 23 illustrates the comprehensive counterrotating vortex and upwash fountain for the condition $H/d = 1$, $Re = 6750$, and $c/d = 3.33$.

Craft et al.⁷⁴ presented computational results for circular jets' flow and heat transfer characteristics arranged in a row (five jets per row) on a semicircular concave surface. They noted that using the standard wall function underestimates heat transfer levels around the stagnation zone and fails to capture secondary Nusselt number peaks associated with jet

downwash flows. They proposed using a differential stress model to simulate the complicated strain fields produced by jet collisions and interactions.

Fregeau et al.⁶⁹ conducted a numerical study using fluent for a simulating single row of jets impinging on the concave surface. They used one equation S-A turbulence models along with the wall function approach. They validated the numerical results with the available data in the open literature and with their previous work data. They observed a significant increase in local Nusselt number distribution along the curvature, with a decrease in jet-to-surface distance. On the other hand, with the rise in jet-to-surface distance, there was a significant reduction in the Nusselt number in the longitudinal direction.

Jung et al.⁷⁵ investigated the effect of changing the injection angle so that the jet strikes the target plate not typically. The study was carried out for staggered array impinging jets in a showerhead cooling system. The jet impinges at an angle on the target surface, as shown in Figure 24. The angled jets heat transfer characteristics were compared with the normal jets and angled jets enhanced the heat transfer compared with the normal jets. The inclined jets overcame the low heat transfer coefficient in the region of center row of holes due to staggered array and curvature effect. This is because of flow imbalance which caused the amount of wall jet to flow towards the low heat transfer region for angled jets.

Bolek and Bayraktar⁷⁶ numerically studied the flow and heat transfer characteristics of a circular jet impinging on three different shaped target surfaces, such as rectangular plate and concave and convex hemispheres. The transitional SST $\kappa-\omega$ turbulence model is used for all flow simulations. The maximum heat transfer is obtained for rectangular plates compared with the hemispheres in the region of stagnation point to the edge of the surfaces. However, in the wall jet region, the convex hemisphere surface has shown maximum heat transfer, and the concave surface showed minimum. Among all the three jets to plate distances ($H/d = 2, 6$, and 9), $H/d = 2$ has demonstrated the highest heat transfer rate in the stagnation region. Figure 25 shows the temperature distribution and streamlines around three different configurations at $H/d = 2$ and $Re = 7043$.

The summary of literature including the method of investigation and techniques used both experimental and numerical are tabulated as shown in Table 7.

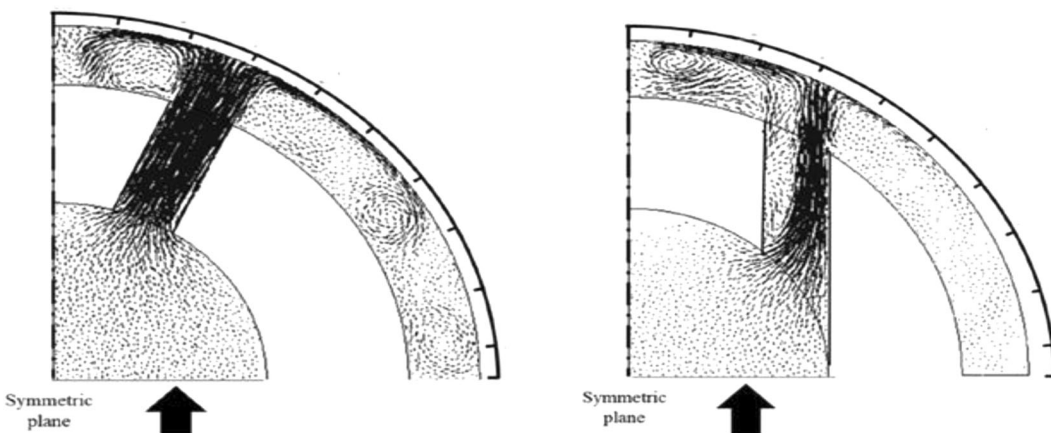


FIGURE 24 Velocity vector plot for normal jet (left) and inclined jet (right)⁷⁵

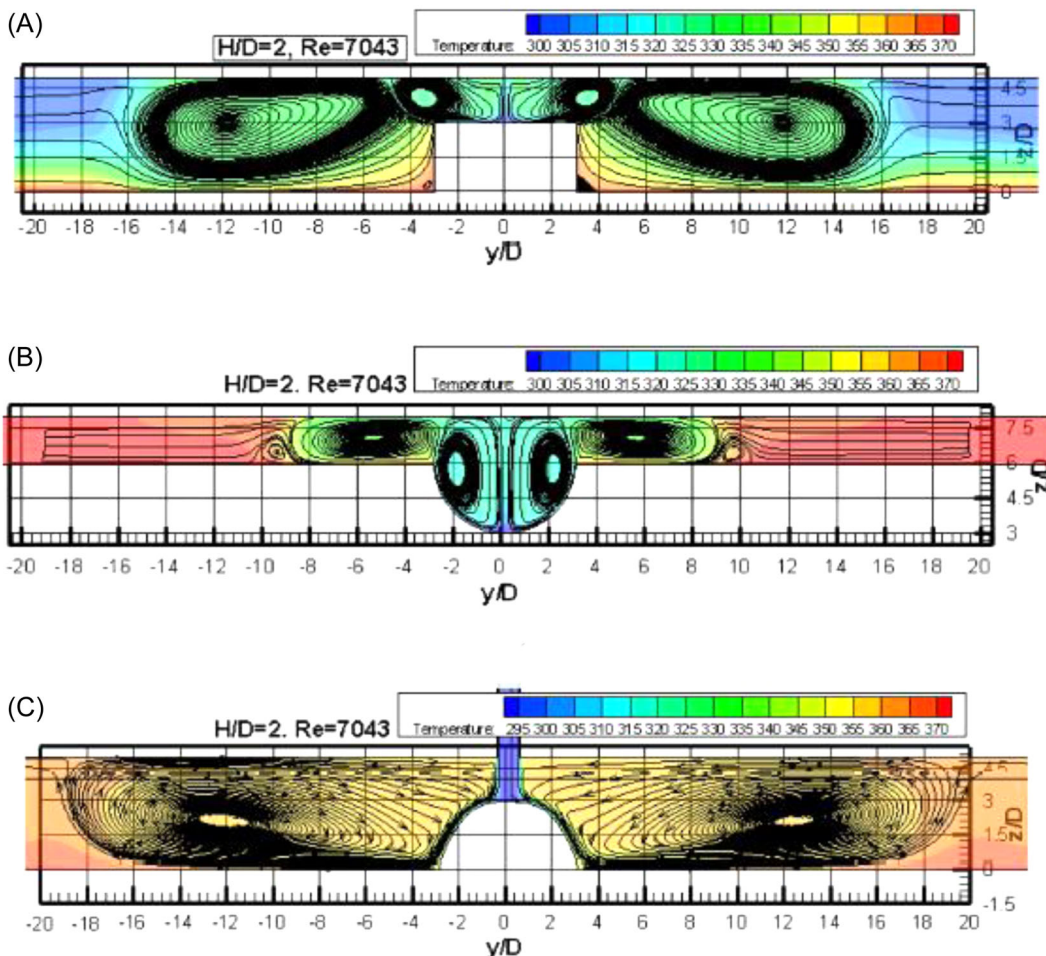


FIGURE 25 Temperature contours in K and streamlines around (A) rectangular plate, (B) concave hemisphere, and (C) convex hemisphere at $H/d = 2$ and $Re = 7043$ ⁷⁶ [Color figure can be viewed at wileyonlinelibrary.com]

3.2 | Flow and heat transfer studies of impinging jets on curve plate with effusion and film holes

Metzger and Bunker⁷⁷ revealed that local heat transfer occurred in the leading-edge region of the airfoil via impingement cooling and film coolant extraction. Experiments were conducted on large-scale models of the turbine vane's leading-edge areas. Their findings indicate that heat transfer is predominantly determined by the Reynolds number of jets, with minor contributions from the flow extraction rate. Additionally, the results suggest that significant changes in leading-edge metal temperatures are feasible by adjusting the spanwise alignment of the impingement nozzles relative to the film-cooling holes. They found that film extraction produced a higher spanwise average Nusselt number over most of the leading edges than the values without film extraction. The impingement locations also moved forward from that without film extraction. The authors attributed these changes to modification of the recirculate

TABLE 7 Summary of literature on jet impingement cooling on curve plate

Authors and year	Geometry	Parameters considered	Method of investigation	Technique used	Remarks
Chupp et al. (1969) ⁶⁰	Curved surface with jet impingement	Jet hole diameter: 0.15–0.6604 mm; Jet hole spacing: 0.79–3.175 mm; Reynolds number: 3000–15,000	Experimental	Electric resistance of platinum strips	They reported correlations for heat transfer along the stagnation line and average heat transfer over the leading-edge portion of target surface
Metzger et al. (1969) ⁶¹	Curved surface with jet impingement	Jet hole diameter: 0.762–1.524 mm; Jet hole spacing: 6.67 d ; Reynolds number: 1150–5500	Experimental	Self-balancing potentiometric recorder; low mass nichrome heater	It was found that the lines of circular jets impinging on the concave surface produced higher heat transfer rates compared with the equivalent two-dimensional slot jets
Tabakoff and Clevenger (1972) ⁶²	Curved surface with jet impingement with three different configurations, namely, slot jet, round jet, and an array of round jets	Circular jet hole diameter: 6.35 mm; Jet hole spacing: 15.8, 31.75, and 55 mm; Jet-to-plate spacing: 1 D ; Reynolds number: 1150–5500	Experimental	250 W strip heater	A single row of smaller jets with larger spacing-to-diameter ratio (c/d) produced the highest heat transfer. A slight increase in overall heat transfer is reported with a change in jet position from the center of symmetry towards the side
Bunker and Metzger (1990) ⁶⁵	Curved surface with jet impingement	Pitch-to-jet diameter ratios: 4.67, 3.33, and 0; Jet Reynolds number: 6700–10,200; Jet nozzle-to-airfoil apex distance: 18 b –36 b	Experimental	Melting pattern of coatings (to determine local surface heat transfer)	They found that close nozzle-to-apex spacing and higher radius ratios are desirable for improved leading-edge heat transfer

(Continues)

TABLE 7 (Continued)

Authors and year	Geometry	Parameters considered	Method of investigation	Technique used	Remarks
Taslim et al. (2001) ⁶⁶	Curved surface with jet impingement with four kinds of walls: (i) smooth wall, (ii) wall with high surface roughness, (iii) wall with conical bumps, and (iv) wall with tapered radial ribs	Jet hole diameter: 8.2 mm; Jet hole spacing: 32.5 mm; Jet-to-plate spacing: 5.2d and 6.2d	Experimental	Thermocouples and pressure taps; contact micromanometer	The conical bumps produced the highest (about 40%) heat transfer enhancement among the four tested surfaces. They reported enhanced heat transfer by roughening the target surface
Nirmalan et al. (2003) ⁶⁷	Elliptic airfoil with Impingement cooling	Jet hole diameter: 1.27 mm; Jet hole spacing: 5d; Jet-to-plate spacing: 1.6d; Jet Reynolds number: 16,636	Experimental	Infrared thermography	Proposed a new technique which makes it possible for the accurate quantification of full-surface internal heat transfer coefficient distributions for prototype
Iacovides et al. (2005) ⁶⁸	Rotating curved surface with jet impingement	Jet hole diameter: 11.2 mm; Jet hole spacing: 44 mm; Jet-to-plate spacing: 35 mm; Jet Reynolds number: 15,000	Experimental	Liquid crystal technique; laser Doppler anemometry	Rotation reduces the heat transfer and disappearance of the secondary peaks
Fenot et al. (2008) ⁷¹	Hot round jets impinging a concave surface	Jet hole diameter: 11.2 mm; Jet hole spacing: 8d; Jet-to-plate spacing: 2–5d; Jet Reynolds number: 10,000 and 23,000	Experimental	Thin heat foil method; Infrared thermography	Heat transfer was found to have enhanced near the impingement zone for large values of relative curvature

TABLE 7 (Continued)

Authors and year	Geometry	Parameters considered	Method of investigation	Technique used	Remarks
Hong et al. (2008) ⁷²	Heat/mass transfer characteristics on a concave surface for stationary and rotating impinging jets	Jet hole diameter: 10 mm; Jet hole spacing: $3d$; Jet-to-plate spacing: $3d$; Jet Reynolds number: 5000	Experimental	Naphthalene sublimation technique	Compared with the flat surface, the heat/mass transfer on the concave surface was enhanced with increasing spanwise direction due to the curvature effect
Ramakumar and Prasad (2008) ⁷³	Single row of circular jets impinging on a semicircular concave surface	Jet hole diameter: 10 mm; Jet hole spacing: 3.33d and 4.67d; Jet-to-plate spacing: $1d$, $3d$, $4d$; jet Reynolds number: 2847–19,300	Computational	$\kappa-\omega$ turbulence model	Higher heat transfer coefficients are obtained when $H/d = 1$ compared with $H/d = 3$ and 4
Jung et al. (2018) ⁷⁵	Jets impinging with an injection angle on showerhead region	Injection angle 25° with normal $H/d = 1$ and hole diameter 5 mm, $Re = 3000$ –10,000	Experimental and computational	Naphthalene sublimation method; shear stress transport (SST) $\kappa-\omega$ turbulence model	High heat transfer rate for angle jets compared with normal jets
Bolek and Bayraktar (2019) ⁷⁶	Circular jet impingement on three different target plates (rectangular, concave, and convex)	Jet-to-plate spacing ratio (H/d) = 2, 6, and 9; Reynolds number = 4276–23,000	Computational	SST $\kappa-\omega$ turbulence model	The maximum heat transfer is obtained for the rectangular plate. In the wall jet region, the convex hemisphere surface has shown maximum heat transfer, and the concave surface showed minimum

region in the leading edge when the jet holes and the bleed holes are inline; bleed flow increases heat transfer. The decrease in heat transfer was reported when the jet holes and bleed holes were 180° out of phase. Figure 26 shows the typical test apparatus that is used for the experiments.

Taslim et al.⁷⁸ experimentally studied the effect of the presence of film holes on a roughened airfoil leading edge. They considered a curved target surface, roughened by the presence of smaller conical bumps and a row of leading-edge film holes. They investigated different flow arrangements and jet Reynolds numbers to conclude that the heat transfer coefficient increases due to the presence of film holes. They found a 35% increase in heat transfer in the leading-edge region due to a conical bump compared with the smooth target surface.

Taslim and Khanicheh⁷⁹ experimentally investigated the heat transfer characteristics of leading-edge impingement with and without showerhead and gill film and its effect on the heat transfer coefficient on the airfoil nose. They varied the jet Reynolds at an elevated range of 8000–48,000. They concluded that the presence of showerhead film holes along the leading edge enhanced the internal impingement heat transfer coefficient significantly. Their numerical result shows an average difference of 10% from the experimental results for no-shower head flow and 30% for showerhead flows.

Ashok Kumar and Prasad⁸⁰ reported the computational investigation on a curved plate with five rows of circular impinging jets and four rows of effusion holes. They studied the effect of exit configurations spent air along with the different arrangements of jet orifices and effusions hole for a constant mainstream Reynolds number (7500). They found the first and second peaks in the Nusselt number due to an increase in turbulence produced around the nozzle edge and the formation of the second stagnation zone, respectively.

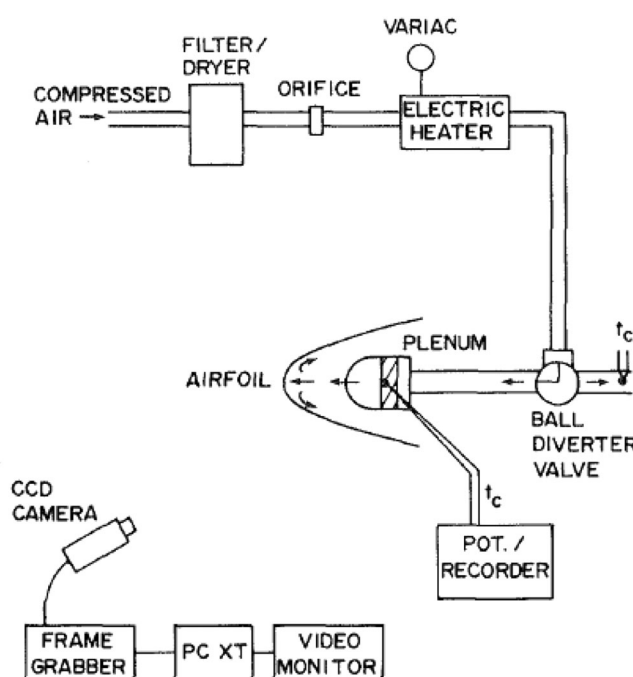


FIGURE 26 Schematic of the test apparatus without film-cooling extraction⁷⁷

3.3 | Conjugate heat transfer studies on curve surface

Albert et al.⁸¹ carried out studies on vane leading-edge regions for different materials in such a way that the external and internal heat transfer coefficients represent the actual engine condition. They named this scaling the matched Biot number method and reported considerable variation in the adiabatic and overall cooling effectiveness.

Kusterer et al.^{82,83} stress the importance and improvement in predicting three-dimensional thermal loads by using conjugate techniques. All the numerical results were compared against the thermal index paint measurements. Their measurements and calculations recommended conjugate calculations to detect regions of the high thermal load for the design of the cooling configuration. The comparison is shown in Figure 27.

Ravelli et al.⁸⁴ studied the conjugate effect computationally by considering a leading-edge geometry. They demonstrated that internal impingement cooling enhances overall effectiveness.

Nathan et al.⁸⁵ investigated the adiabatic and overall effectiveness of an internal impingement-cooled vane's leading-edge section. They reported that internal impingement leads to higher overall effectiveness than adiabatic effectiveness. They emphasized the usage of overall effectiveness distribution to predict the hot spot on vane surfaces.

Montomoli et al.⁸⁶ considered the impingement on a cylindrical plate made from materials of different thermal conductivities to probe the effect of conduction on cooling effectiveness. They considered two materials, polycarbonate and stainless steel, to highlight the impact of conduction on coolant effectiveness. They found lower thermal gradients for higher conducting

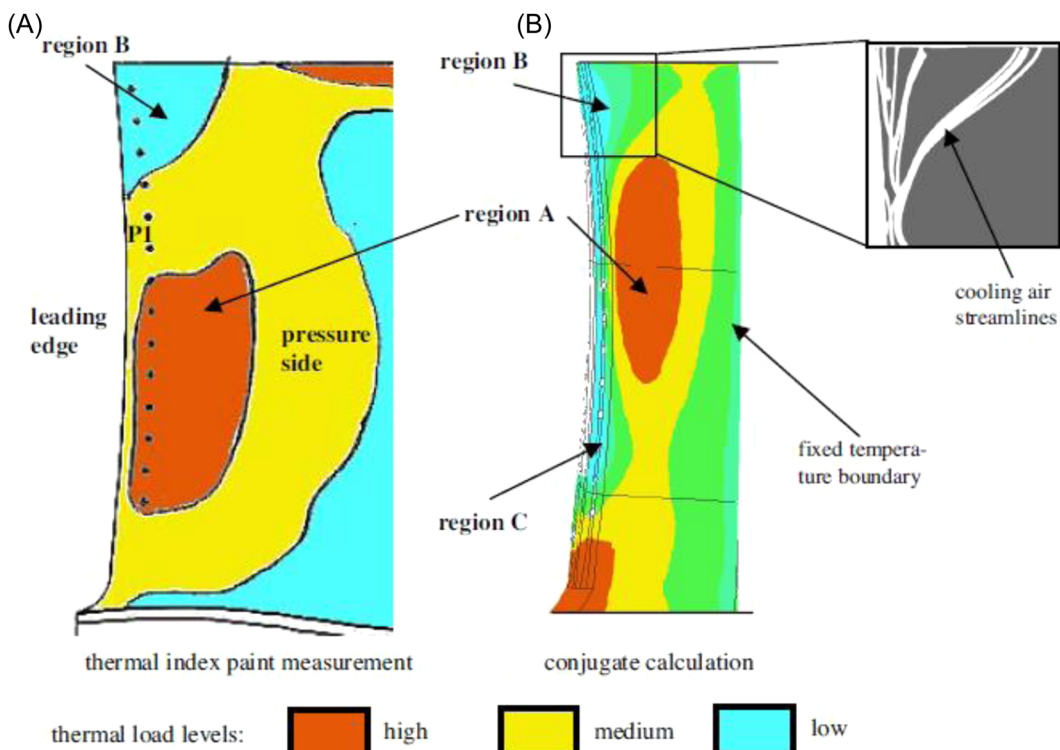


FIGURE 27 Comparison of thermal index paint measurement and conjugate calculation of leading-edge region (pressure side)⁸³ [Color figure can be viewed at wileyonlinelibrary.com]

material. They emphasized the importance of uniform effectiveness distribution in reducing the thermal stress and also stated that using inserts of nickel-aluminide alloys in nozzles reduced thermal gradients from 3 to 4 times compared with current designs.

Chandran and Prasad⁸⁷ have studied leading-edge heat transfer computationally and experimentally typical gas turbine NGV cooled by a combination of impingement and showerhead film cooling. They revealed the complex flow structure owing to the coolant–mainstream interaction and the influence of vane material thermal conductivity. They observed that overall effectiveness is strongly dependent on vane material conductivity.

Lamani⁸⁸ conducted computational studies for NGV leading edge with effusion holes and multiple jet impingements under conjugate boundary conditions for different materials (steel, nickel, inconel, and titanium). They found that heat flux is more for Inconel material, and strength is more for Inconel material. But the Inconel's density is higher than the other three materials.

The summary of literature including the method of investigation and techniques used in both experimental and numerical are tabulated as shown in Table 8.

4 | CONJUGATE HEAT TRANSFER STUDIES ON AIRFOIL SURFACE

4.1 | Effect of material thermal conductivity on film-cooling effectiveness

Heidmann et al.⁸⁹ used a solver that coupled the in-house Glenn-HT fluid convection solver with the Boundary Element Method for solid conduction in their conjugate calculation of a realistic film-cooled turbine vane. They presented results with high thermal conductivity and low thermal conductivity vane cases. They pointed out the importance of adopting a three-dimensional conduction equation for conjugate problems with film cooling.

Mazur et al.⁹⁰ studied the steady-state conjugate heat transfer effect computationally for a first-stage nozzle guide vane. Their main focus was to predict the temperature distribution on the nozzle vane. They concluded that varying the cooling airflow rate significantly affects the temperature distribution for the solid nozzle body. The temperature distribution for nozzle vane pressure surface and shrouds is shown in Figure 28.

Dees et al.⁹¹ presented experimental surface temperature measurements on the suction side of a film-cooled scaled-up turbine vane model. They conducted the experiments using two different conductivity vane models to represent adiabatically ($k = 0.048 \text{ W/m K}$) and conjugate ($k = 1.02 \text{ W/m K}$) conditions. They reported the contribution of film cooling in the overall effectiveness by comparing it with their earlier work⁹² that was carried out with only internal cooling with the U-bend channel. They concluded that the addition of film cooling decreased the overall surface temperature. However, for a particular momentum flux ratio, the increased surface temperature was observed due to the detached film coolant flow.

Albert and Bogard⁹³ compared the performance of normal cylindrical holes with trenched cooling holes on the pressure side of a turbine vane. They measured adiabatic and overall effectiveness at various blowing ratios and reported that the increase in blowing ratio improved overall effectiveness. The increasing blowing ratio reportedly adversely affected the pressure side with normal cylindrical holes due to coolant getting lifted off from the surface.

TABLE 8 Summary of literature on jet impingement cooling on the curved plate with effusion and film-cooling holes and other conjugate studies

Authors and year	Geometry	Parameters considered	Method of investigation	Technique used	Remarks
Metzger and Bunker (1990) ⁷⁷	Jet impingement cooling on the curved plate with effusion holes	Pitch-to-jet diameter ratios: 4.67, 3.33, and 0; Jet Reynolds number: 6700–10,200; Jet nozzle-to-airfoil apex distance: –18b to 36b	Experimental	CCD camera; melting pattern of coating	Their result shows that the heat transfer primarily depends on jet Reynolds number with smaller influences from the flow extraction rate
Taslim et al. (2001) ⁷⁸	Jet impingement cooling on a roughened curved plate with film holes	Jet hole diameter: 8.2 mm; Jet hole spacing: 32.5 mm; Jet-to-plate spacing: 5.2d and 6.2d; Jet Reynolds number 13,500–36,000	Experimental	Thermocouples, micromanometer, unigraphics, laminated object model for casting	Concluded that heat transfer coefficient increases due to the presence of film holes. They also reported a 35% increase in heat transfer due to the presence of a conical bump compared with the smooth target surface
Taslim and Khanicheh (2006) ⁷⁹	Jet impingement cooling on the curved plate with and without showerhead and gill film holes	Jet hole spacing: 61.7 mm; Jet-to-plate spacing: 2.8d; Jet Reynolds number 8000–48,000	Experimental and computational	Contact micromanometer, venturimeter, foil heaters, high Reynolds number κ - ϵ turbulence model	They concluded that the presence of showerhead film holes along the leading edge enhances the internal impingement heat transfer coefficient significantly. Their numerical results show an average difference of 10% from the experimental results for no-shower head flow and 30% for showerhead flows
Ashok Kumar and Prasad (2011) ⁸⁰	Jet impingement cooling on the	Jet hole diameter 5 mm; jet hole spacing: 5.4d; Jet Reynolds number 7500	Computational	Shear stress transport (SST) κ – ω turbulence model	They found out the first and second peaks in Nusselt number due to an increase in

(Continues)

TABLE 8 (Continued)

Authors and year	Geometry	Parameters considered	Method of investigation	Technique used	Remarks
	curved plate with effusion holes	four different spent exit configurations			turbulence produced around the nozzle edge and the formation of the second stagnation zone, respectively
Ravelli et al. (2010) ⁸⁴	Jet impingement cooling on the curved plate with film holes with conjugate effects	Jet hole diameter 5 mm and 3.5 mm; Jet-to-plate spacing: 28.2 mm; Blowing ratios 1 and 2; Conductivity: 0.041, 1.01, and 202 W/m K	Computational	Realizable $\kappa-\epsilon$ turbulence model	They showed that the overall effectiveness was slightly improved by the impingement cooling. This small effect on overall effectiveness was shown to be due to conjugate effects, including a reduction of convective cooling within the coolant holes when impingement cooling was used
Nathan et al. (2012) ⁸⁵	Jet impingement cooling on curved vane leading edge with showerhead film holes	Blowing ratios 0.4 and 1.2; Conductivity: 0.048 and 1.1 W/m K	Experimental	IR thermography; Matched Blot number method	They concluded that due to the internal impingement cooling, overall cooling effectiveness values were significantly higher than the adiabatic film effectiveness values
Chandran and Prasad (2015) ⁸⁷	Jet impingement cooling on curved vane leading edge	Jet hole diameter: 5 and 3.5 mm; Jet-to-plate spacing: 1.2d; Blowing ratios: 1, 1.5, and 2;	Experimental and computational	IR thermography; SST $\kappa-\omega$ turbulence model	They revealed the complex flow structure owing to the coolant-mainstream interaction and the influence

TABLE 8 (Continued)

Authors and year	Geometry	Parameters considered	Method of investigation	Technique used	Remarks
	with showerhead film holes	Conductivity: 0.2 and 14.9 W/m K; Mainstream Reynolds number: 4.8×10^5 – 14.4×10^5	Jet diameter 2.5 mm; film-cooling hole diameter: 2.85 mm; Distance b/w target plate and jet 2.8 mm; Main stream Reynolds number: 41,855; Jet $Re = 4350$	Computational	SST $\kappa-\omega$ turbulence model Heat flux is more for Inconel material among steel, inconel, titanium, and nickel
Lamani et al. (2017) ⁸⁸	Curved plate of a leading-edge region of nozzle guide vane				

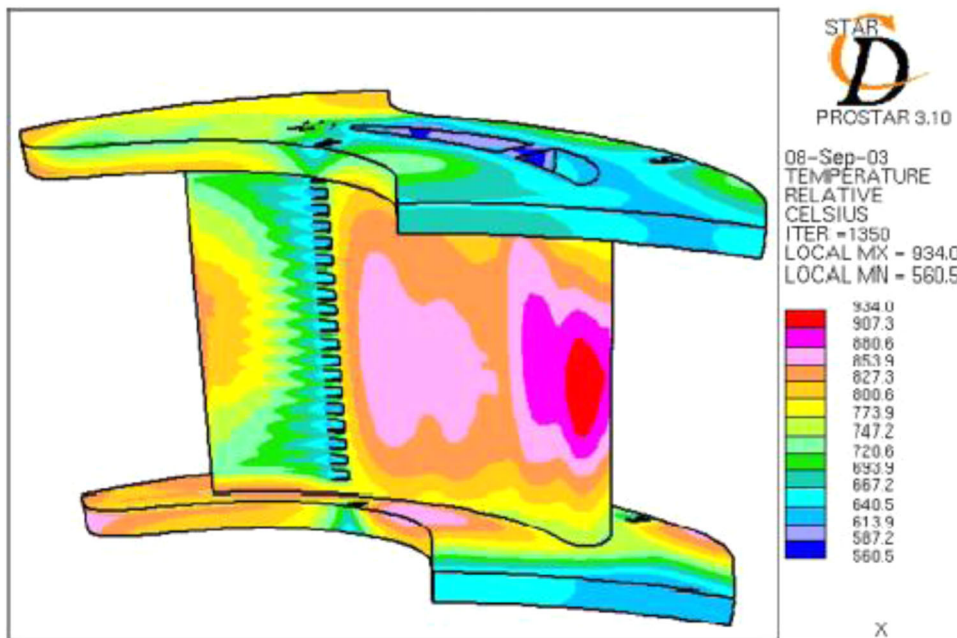


FIGURE 28 External surface temperature distributions on the nozzle vane pressure side and shrouds⁹⁰
[Color figure can be viewed at wileyonlinelibrary.com]

Williams et al.⁹⁴ investigated the overall cooling effectiveness of a turbine airfoil surface equipped with internal impingement cooling. They conducted studies comparing the effects of internal cooling alone to those of film and internal cooling. Their findings indicated that the enhanced performance associated with increasing the momentum flux ratio was attributable to a compensating increase in the internal cooling provided by the impingement jets. They concluded that as the momentum flux ratio increases, the adiabatic effectiveness falls, although the overall cooling effectiveness increases.

In the above studies of Bogard and co-workers^{91–94} the matched Biot number method was used for cooled NGV. They noted that because the laboratory experiment is conducted at temperatures and pressures substantially lower than those encountered in real engines, the dimension temperature, and heat transfer coefficient values are lower. Thus, to match the laboratory-derived normalized surface temperature values to those of the actual engine, it is critical to choose a material with lower conductivity. They reported that to simulate the nominal engine condition, the Biot number range should be within 0.4–1.6 for the laboratory experiments.

Pujari et al.⁹⁵ investigated the internal heat transfer coefficient and temperature distribution within a linear cascade of high-pressure nozzle guide vanes. They evaluated a combination of impingement and film cooling and conducted liquid crystal tests to anticipate the internal temperature distribution of the NGV. Considering the conjugate effect shows the effect of material conductivity on average Nu number distributions. Figure 29 shows the temperature contours of film-cooling distributions at the center plane for different mainstream Reynolds' numbers.

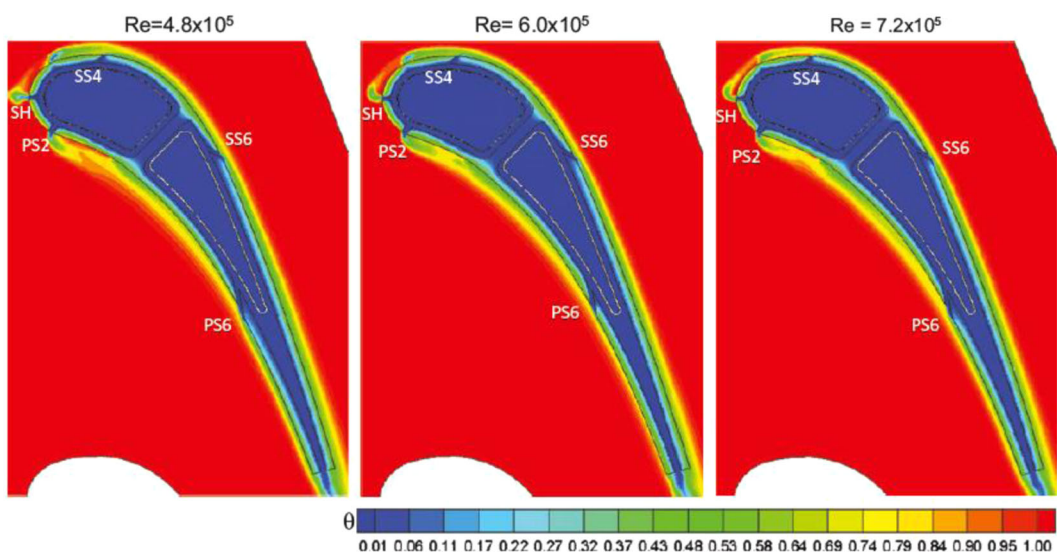


FIGURE 29 Center plane temperature contours showing the effect of mainstream Reynolds number on film coolant distributions⁹⁵ [Color figure can be viewed at wileyonlinelibrary.com]

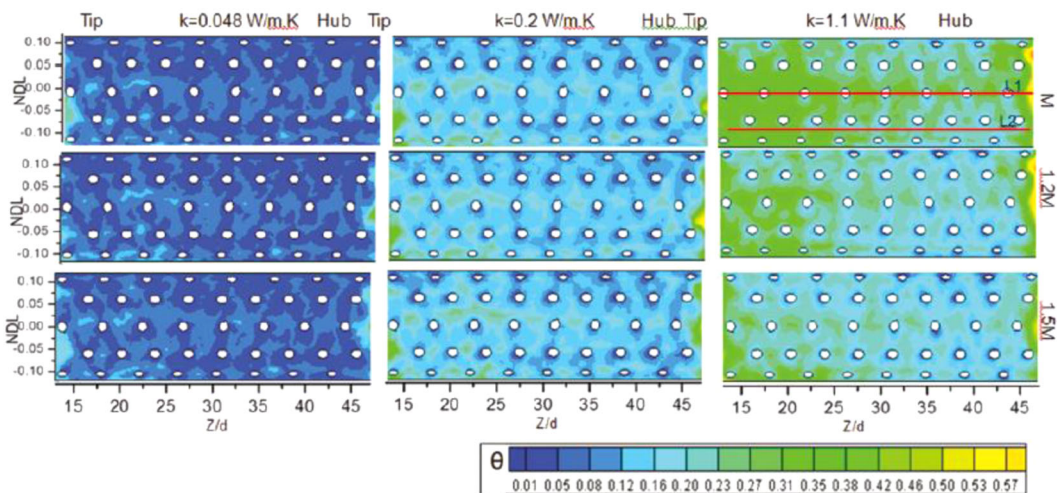


FIGURE 30 Conductivity's effect on the leading-edge region's local surface temperature distribution⁹⁶ [Color figure can be viewed at wileyonlinelibrary.com]

Pujari et al.⁹⁶ examined the effect of thermal conductivity on the internal surface temperature distributions of a nozzle guide vane with impingement and film cooling combined. A higher thermal conductive material is advisable to reduce the thermal stress because of temperature gradients on the vane surface. According to Figure 30, materials with a higher thermal conductivity exhibit a more uniform interior surface temperature distribution, but at a higher temperature, this is because the external surface of the film has lower cooling effectiveness.

Pujari⁹⁷ performed conjugate heat transfer analysis on an NGV equipped with impingement and film-cooling holes. The effect of mainstream and coolant mass flow rate on the internal surface temperature distribution is studied, and they are affected differently in different regions of NGV. He concluded that generalized geometries might not yield accurate results for obtaining the internal surface temperature distributions in forecasting the nozzle guiding the vane's life.

From the study of conjugate heat transfer on an airfoil previously, it is clear that most of the published research focused on comparing the adiabatic and conjugate effectiveness distribution on the external surface. Few of them incorporated the internal impingement cooling configuration with film-cooling holes for the conjugate study. However, their main focus was to address the external effectiveness. Only a few researchers addressed the internal impinging target surface heat transfer phenomena under adiabatic and conjugate conditions though many of them stated that enhancing the internal cooling causes a decrease in the metal temperature.

4.2 | Conjugate heat transfer studies

Usually, gas turbine vanes are exposed to very high-temperature gases to obtain maximum efficiency from the gases. But metallurgical considerations limit the operating temperature and necessitate the study of heat transfer distribution not only in the gases or fluids but also in the blades or solids. A study of wall temperature distribution in solids is also necessary for the selection of the material. Hence conjugate heat transfer problem comes into the picture, which solves the energy equation of the solid along with fluid flow equations. In a nonconjugate problem, the temperature distribution in the boundary layer of the mainstream is determined under a prescribed condition at the surface, and then the heat transfer coefficient is calculated. Next, the heat transfer process in the solid is calculated. Thus, a predetermined heat transfer coefficient describes the complexity of the heat transfer processes between the solid and the mainstream, demonstrating that the heat transfer process is independent of the solid properties. Contrarily, conjugate heat transfer calculates fluid and solid heat transfer characteristics simultaneously. Hence convective heat transfer problems with conjugate heat transfer seem to be more realistic compared with the other.

Figure 31 shows the nondimensional temperature distribution (θ r.m.s.) around a cylinder for both conjugate and adiabatic conditions. The θ r.m.s. at the interface for the conjugate condition are less due to the higher heat conduction in the solid compared with the adiabatic condition.

5 | OTHER GEOMETRICAL AND FLOW CONFIGURATIONS

5.1 | Effect of rotation on the impinging jet in rectangular channels

Parsons and Han,⁹⁹ Parsons et al.,¹⁰⁰ and Akella and Han¹⁰¹ investigated the effect of rotation on jet impingement heat transfer by the inline array of circular jets in smooth rectangular channels on heated target walls. No change in the pressure and flow distribution was observed for cases with and without rotation for a jet Reynolds' number. They also concluded that there

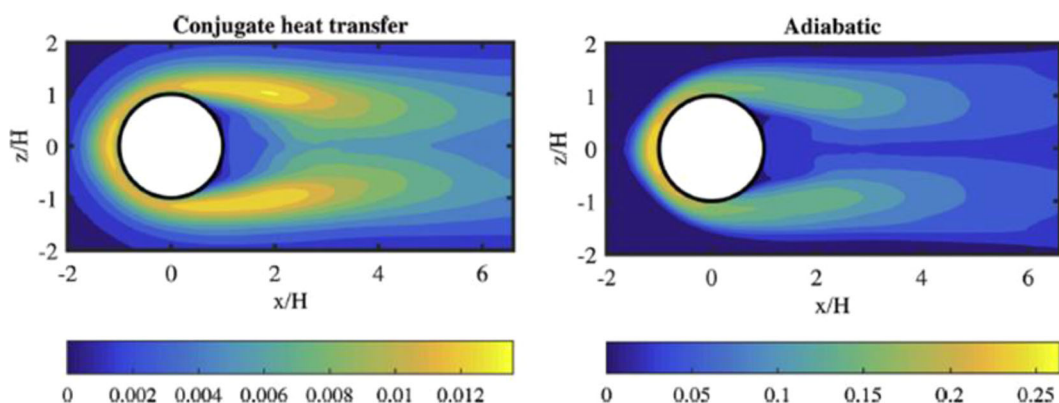


FIGURE 31 Nondimensional temperature θ r.m.s. on the fluid–solid interface in conjugate heat transfer (left) and adiabatic (right) cases⁹⁸ [Color figure can be viewed at wileyonlinelibrary.com]

was a decrease in the heat transfer due to the rotation of the channel compared with the nonrotating condition, as the rotational effect causes the induction of secondary flows, which deflects the impinging jets. The deflection of the jets is due to the centrifugal forces, Coriolis components, and buoyancy effects.

Akella and Han¹⁰² studied the effect of rotation for a two-pass rectangular channel with ribbed target walls. They compared the pressure distribution and other heat transfer parameters with the walls without ribs. According to the results, the ribbed walls with rotation have increased heat transfer from 9% to 44%, with an increase in jet Reynolds' number from 4×10^3 to 1×10^4 . However, they also observed that 20% of the heat transfer coefficient decreased due to the rotation compared with nonrotation. Forward rotation tests showed a slightly higher average Nu number than reverse rotation.

Following previous studies on rotational effects on jet impinging heat transfer for rectangular channels, Parsons and Han¹⁰³ further investigated the rotational effect with film coolant extraction. In the present study, the target wall was modified with film extraction holes to extract the spent air after impingement. The film extraction holes decreased the effect of cross-flow on other jets. So there was an increase in the heat transfer observed for the target wall with film extraction holes. Also, the rotation significantly affects leading channel target walls more than trailing channel target walls.

Parsons and Han¹⁰⁴ also worked on the staggered film coolant extraction to investigate the rotational effect on jet impingement heat transfer by placing the jet holes and target film extraction holes in a staggered manner. They concluded that no difference was observed with the staggered pattern compared with the previous study.

5.2 | Effect of the roughness of the target plate on heat transfer

Azad et al.¹⁰⁵ studied the effect of dimples placed on the target surface using the transient liquid crystal technique on heat transfer enhancement. As shown in the figure, three different cross-flow orientations were created and studied by changing the exit flow conditions of the test setup. Cross-flow exit direction 2 showed higher heat transfer enhancement than other directions. There was no change in the Nu number for the cases with and without dimple

surfaces. But, the dimpled surface showed higher heat transfer due to increased circumferential area.

Azad et al.¹⁰⁶ also investigated by placing the pins instead of dimples on the target surface for the same three cross-flow orientations as in the previous study with the same test setup. The exit directions 1 and 2 have the same and higher heat transfer enhancement compared with exit direction 3 for the pinned surface. The directions are the same as the dimpled surface shown in Figure 32. They also concluded that there was no difference in the averaged impingement heat transfer coefficient with fewer pins and more pins study.

From the above two studies, the dimpled surface can be advantageous over the pinned surface by considering material cost and weight factor.

Rallabandi et al.¹⁰⁷ studied the effect of roughness created by placing the axial ribs (staggered and inclined) and porous aluminum foam on a rectangular channel under the impinging jet and through channel flow conditions. There is a significant increase in heat transfer and drop in pressure observed for all the cases compared with the smooth surface. However, the increase in heat transfer in axial ribs is much lower than the channel with perpendicular or skewed ribs reported in the literature. Axial ribs, through flow cases, showed lower pressure drop than the perpendicular or skewed ribs in channel flow from the literature. Staggered ribs offer a higher friction factor than inclined ribs. Impinging jets provide much higher heat transfer at a pressure drop cost than axial ribs' channel flow. Finally, compared with all the cases, porous foam surface has shown better performance in terms of heat transfer, and porous foam with jet impingement resulted in less pressure drop compared with axial ribs.

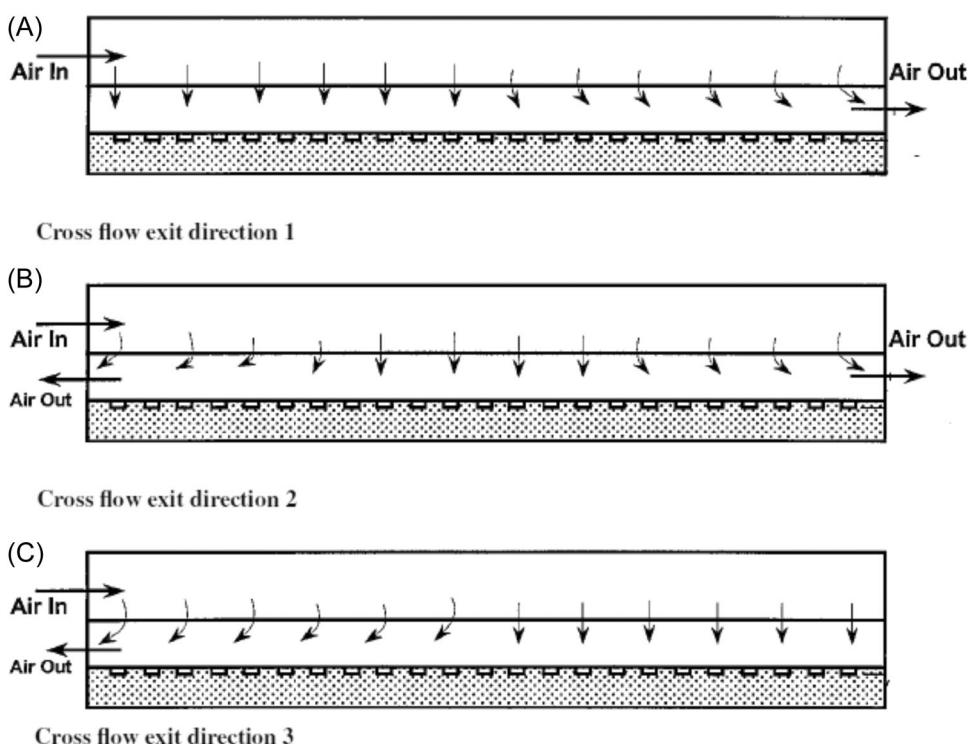


FIGURE 32 Impingement target surface with different cross-flow directions for dimple surface¹⁰⁶

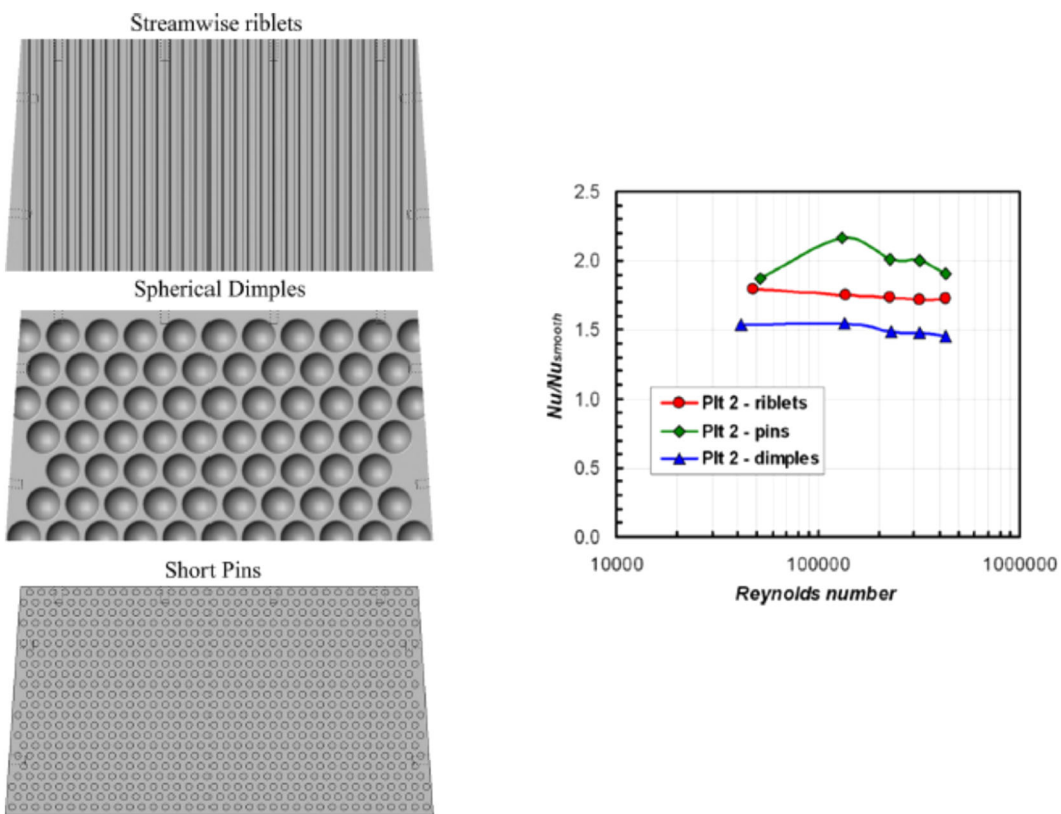


FIGURE 33 Different turbulated target walls (left) and nondimensional Nu variation with the Re number (right).¹⁰⁸ [Color figure can be viewed at wileyonlinelibrary.com]

Mhetras et al.¹⁰⁸ experimentally investigated the effect of different turbulated target wall configurations such as streamwise riblets, short pins, and spherical dimples for a jet impingement array on heat transfer and pressure drop. A wide range of Reynolds numbers (50,000–450,000 (based on average jet hole diameter)) are used for the experimental investigations. Two jet plate designs are used, one with increasing hole diameter (Plt 1) and another with decreasing hole diameters (Plt 2) in streamwise directions. The increasing hole diameter design has shown more heat transfer gradients with low magnitude compared with the decreasing hole diameters design. However, losses are less for the latter case. The short pins target wall configuration has given the highest heat transfer enhancement based on the average Nu distributions compared with the other two configurations for all Reynolds' numbers. Figure 33 shows the geometric and Nu variation for the different target walls.

6 | CONCLUSION AND FUTURE SCOPE

The review of the preceding literature gives a detailed picture of jet impingement internal cooling under different boundary conditions on a flat plate, curved plate, and airfoil surface. Both numerical and experimental investigations have shown the impact of jet impingement cooling for high convective heat transfer rates compared with other cooling techniques.

Different types of jet configurations such as slot jet, round jet, single row, and an array of round jets are reported in the literature for both flat and curved plates. The conclusions from the preceding literature review are presented as follows

1. Many of the authors concluded that the local value of internal surface temperature and heat transfer coefficient are strong functions of local flow behavior. The flow behavior is greatly influenced by different geometric variations. Therefore, conventional methods of obtaining the internal temperature distributions and internal heat transfer coefficient by considering generalized geometries like the flat and curved plate may not yield accurate solutions.
2. Extensive computational studies were reported on flat and curve plate jet impingement heat transfer. In these studies, most of the previous research recommended the usage of $\kappa-\omega$ SST and $\kappa-\varepsilon$ realizable turbulence models for jet impingement heat transfer problems.
3. From the literature survey, it is observed that the jet impingement cooling flow and heat transfer behavior in the presence of pedestal and ribs is not explored extensively. This may be due to the fact that impingement cooling with ribs and pedestals may lead to higher pressure drop.
4. Very limited studies were found in the literature which considered realistic cooling configurations, that is, NGVs with combined internal and external cooling. Among the available research on nozzle guide vanes, most of them considered either film cooling or jet impingement cooling. However, very few of them considered internal impingement cooling for a film-cooled vane.
5. Researchers who carried out conjugate heat transfer studies on NGV point out the importance of conjugate thermal considerations in the accurate prediction of heat transfer in gas turbine blades and vanes. From the conjugate studies, it can be concluded that higher thermal conductive blade material has shown less thermal stress and more life in the vane. Under the conjugate conditions, experimental measurement of the internal surface temperature of a blade is a formidable task and hence may have been avoided by many researchers.
6. It is also observed from the literature that in an actual nozzle guide vane geometry, the flow and heat transfer patterns on the exterior and interior sides vary considerably, and the internal surface temperature is a strong function of the Nusselt number variation. The effect of pressure gradient on the external surface and the effect of cross-flow on the internal side cannot be generalized using a flat or curve plate. Further, it is observed that limited experimental data is available for conjugate heat transfer studies for a typical nozzle guide vane or blade. This unavailability of benchmark data is a constraint in validating the reported computational studies.
7. It is necessary to consider not only heat transfer enhancement but also the pressure drop that occurred due to different roughened target surfaces.

6.1 | Future scope

Studies on nozzle guide vane or gas turbine blades give accurate results compared with flat or curved plates. The effect of pressure gradient on the external surface and the effect of cross-flow on the internal side cannot be generalized using a flat or curve plate. So investigations on aerofoil blades are advantageous. Investigation on hybrid cooling like combined impingement and film cooling shows better heat transfer characteristics compared with individual cooling,

TABLE 9 Summary of literature on jet impingement on aerofoil surface with conjugate studies

Authors and year	Geometry	Parameters considered	Method of investigation	Technique used	Remarks
Heidmann et al. (2003) ⁹⁰	Honeywell film-cooled engine design	Material thermal conductivity (Inconel: 27.7 W/m K, silicon nitride ceramic: 8 W/m K); Exit Reynolds number: 2.9×10^6 ; Temperature of main stream: 1726K; Temperature of coolant: 863 K	Computational	Coupled boundary element method (for conduction); Glenn-HT (for convection); $\kappa-\omega$ turbulence model	Adopted a three-dimensional conduction equation for conjugate problems with film cooling and presented its significance
Mazur et al. (2006) ⁹¹	Single turbine nozzle vane	Parabolic static temperature with maximum temperature of 1085°C, flow velocity: 214–429.3 m/s; coolant velocity: 35.7–286 m/s	Computational	Star CDV3.150A $\kappa-\epsilon$ turbulence model with wall function renormalization group theory	Concluded that varying the cooling airflow rate has a significant effect on the temperature distribution for the solid nozzle body
Dees et al. (2012, 2013) ^{92,93}	C3Xvane profile	Main stream temperature: 300 K; Coolant temperature: 250 K; Main stream Re number: 750,000; Coolant Re number: 10,000–40,000; thermal conductivity of adiabatic test vane k : 0.048 W/m K; Conductive test vane k : 1.02 W/m K; Diameter of film-cooling hole: 4.1 mm Pitch to diameter ratio: 3; Blowing ratio M : 0.64, 0.95, and 1.3	Experimental and numerical	IR camera, Standard $\kappa-\omega$ turbulence model, and shear stress transport (SST) theory	Concluded that the addition of film cooling decreased the overall surface temperature. Detached flow causes a decrease in surface temperature
Albert and Bogard (2013) ⁹⁴	Aerofoil	Main stream temperature: 305 K; Coolant temperature: 220 K; Main stream Re number: 700,000; Coolant Re number: 20,000; Thermal conductivity of adiabatic	Experimental	Matched Bi number method, Infrared thermography	Reported that with the increase in blowing ratio, overall effectiveness is improved, and coolant jet liftoff was observed

(Continues)

TABLE 9 (Continued)

Authors and year	Geometry	Parameters considered	Method of investigation	Technique used	Remarks	
Williams et al. (2014) ⁹⁵	NASA c3x vane	test vane k : 0.048 W/m K; Conductive test vane k : 1.06 W/m K; Diameter of film-cooling hole (d): 4.22 mm; Pitch (centerline to centerline): 5.6 d	Main stream temperature: 305 K; Coolant temperature: 254 K; Main stream Re number: 700,000; Thermal conductivity of adiabatic test vane k : 0.048 W/m K; Conductive test vane k : 1.06 W/m K; Diameter of film-cooling hole (d): 6.35 mm; Pitch to diameter spacing ratio: 4; Momentum flux ratio: 0.18–5	Experimental	Matched Bi number method, Infrared thermography	Concluded that as the momentum flux ratio increases, the adiabatic effectiveness falls, although the overall cooling effectiveness increases
Pujari et al. (2017) ⁹⁶	High-pressure turbine stage nozzle guide vane (NGV)	Main stream Re number: 4.8×10^5 , 6.04×10^5 , and 7.2×10^5 ; coolant Re number: 17,894–74,561; Blowing ratio (M): 1, 1.2, and 1.5; Jet-to-plate space ratio (H/d): 1.2; Main stream temperature: 339 K; Coolant temperature: 288 K; Thermal conductivity: 0.04, 0.2, and 1.1 W/m K	Experimental and computational	Thermochronic liquid crystal technique, MAT LAB, Camcorder	Considering the conjugate effect shows the effect of material conductivity on average Nu number distributions	
Pujari et al. (2018) ⁹⁷	High-pressure turbine stage NGV	Main stream Re number: 4.8×10^5 ; coolant mass flow rate: 0.0015–0.009 kg/s; Blowing ratio	Experimental and computational	Thermochronic liquid crystal technique, MAT LAB, Camcorder	Lower conductive material shows a higher temperature	

TABLE 9 (Continued)

Authors and year	Geometry	Parameters considered	Method of investigation	Technique used	Remarks
Pujari (2019) ⁹⁸	High-pressure turbine stage NGV	Main stream Re number: 1.44×10^5 , 2.4×10^5 , and 3.38×10^5 ; Coolant mass flow rate: $0.0037\text{--}0.0093 \text{ kg/s}$; Blowing ratio (M): 1, 1.2, and 1.5; Jet-to-plate space ratio (H/d): 1.2	Computational	SST $\kappa-\omega$ turbulence model	Concluded that generalized geometries may not yield accurate results in forecasting the nozzle guiding the vane's life
		conductivity: 0.048, 0.2, and 1.1 W/m K			

and much research is needed in hybrid cooling.^{107–118} Experimental works on conjugate heat transfer studies are limited. Considering the secondary flow losses may produce a better understanding of the realistic gas turbine engines (Table 9).

NOMENCLATURE

Bi	Biot number
d, D	diameter of the jet hole, m
h	heat transfer coefficient, W/m ² K
H	distance between the jet hole and target surface, m
K	thermal conductivity, W/m K
L	span length, m
M	mass flow, kg/s
Nu	Nusselt number
q''	heat flux
Re	Reynolds number
T	temperature, K
V	velocity, m/s

GREEK SYMBOLS

μ	coefficient of viscosity, N s/m ²
ω	specific dissipation rate, 1/s
φ	overall effectiveness, $(T_m - T_e)/(T_m - T_c)$
ρ	density, kg/m ³

ORCID

Gudla Babji  <http://orcid.org/0000-0002-7208-0228>

REFERENCES

- Pujari AK. *Internal Heat Transfer Studies in a Gas Turbine Nozzle Guide Vane with Combined Impingement and Film Cooling*. Doctoral Thesis. IIT Madras; 2016.
- Jambunathan K, Lai E, Moss MA, Button BL. A review of heat transfer data for single circular jet impingement. *Int J Heat Fluid Flow*. 1992;13(2):106–115.
- Al-Sanea S. A numerical study of the flow and heat transfer characteristics of an impinging laminar slot-jet including crossflow effects. *Int J Heat Mass Transfer*. 1992;35(10):2501–2513.
- San JY, Huang CH, Shu MH. Impingement cooling of a confined circular air jet. *Int J Heat Mass Transfer*. 1997;40:1355–1364.
- Fitzgerald JA, Garimella SV. A study of the flow field of a confined and submerged impinging jet. *Int J Heat Mass Transfer*. 1998;41:1025–1034.
- Behnia M, Parneix S, Shabany Y, Durbin PA. Numerical study of turbulent heat transfer in confined and unconfined impinging jets. *Int J Heat Fluid Flow*. 1999;20(1):1–9.
- Li CY, Garimella SV. Prandtl-number effects and generalized correlations for confined and submerged jet impingement. *Int J Heat Mass Transfer*. 2001;44(18):3471–3480.
- Koseoglu M, Baskaya S. The effect of flow field and turbulence on heat transfer characteristics of confined circular and elliptic impinging jets. *Int J Therm Sci*. 2008;47:1332–1346.
- Kozlov GV, Grek GR, Sorokin AM, Litvinenko YA. Influence of initial conditions at the nozzle exit on the structure of the round jet. *Thermophys Aeromech*. 2008;15(1):55.
- Alekseenko SV, Dulin VM, Tokarev MP, Markovich DM. A swirling jet with vortex breakdown: three-dimensional coherent structures. *Thermophys Aeromech*. 2016;23(2):301–304.

11. Firdaus M, Khalil M, Musa MN. The effectiveness of jet impingement cooling system on various flat plate surface. *J Biolubricant Eng Sci.* 2019;1(2):1-7. <https://www.fazpublishing.com/jbes>
12. Florschuetz L, Metzger D, Su C. Heat transfer characteristics for jet array impingement with initial crossflow. In: Ayyaswamy PS, ed. *ASME 1983 International Gas Turbine Conference and Exhibit*. Vol 34, No. 106; 1984.
13. Jakubowski AK. Experimental study of the interaction of multiple jets with a cross flow. *AIAA Journal.* 1985;23(11):1679-1683. <https://doi.org/10.2514/3.9151>
14. Van Treuren KW, Wang Z, Ireland PT, Jones TV. Detailed measurements of local heat transfer coefficient and adiabatic wall temperature beneath an array of impinging jets. *ASME J Turbomach.* 1994;116(3): 369-374.
15. Brizzi LE, Bernard A, Bousgarbiès JL, Dorignac E, Vullierme JJ. Study of several impinging jets. *J Therm Sci.* 2000;9(3):217-223.
16. Hwang J-J, Cheng C-S. Impingement cooling in triangular ducts using an array of side-entry wall jets. *Int J Heat Mass Transfer.* 2001;44:1053-1063.
17. Ekkad SV, Pamula G, Acharya S. Influence of crossflow-induced swirl and impingement on heat transfer in an internal coolant passage of a turbine airfoil. *ASME J Heat Transfer.* 2000;122:587-597.
18. Son C, Gillespie D, Ireland P, Dailey GM. Heat transfer and flow characteristics of an engine representative impingement cooling system. *ASME J Turbomach.* 2001;123(1):154-160.
19. Aldabbagh LBY, Sezai I. Numerical simulation of three-dimensional laminar multiple impinging square jets. *Int J Heat Fluid Flow.* 2002;23(4):509-518.
20. Thielen L, Jonker HJJ, Hanjalić K. Symmetry breaking of flow and heat transfer in multiple impinging jets. *Int J Heat Fluid Flow.* 2003;24(4):444-453.
21. Yan W, Mei S, Liu H, Soong C, Yang W-J. Measurement of detailed heat transfer on a surface under arrays of impinging elliptic jets by a transient liquid crystal technique. *Int J Heat Mass Transfer.* 2004;47: 5235-5245.
22. Geers LFG, Tummers MJ, Hanjalić K. Experimental investigation of impinging jet arrays. *Exp Fluids.* 2004;36(6):946-958.
23. Chambers AC, Gillespie DR, Ireland PT, Dailey GM. The effect of initial cross flow on the cooling performance of a narrow impingement channel. *ASME J Heat Transfer.* 2005;127:358-365.
24. Dano BPE, Liburdy JA, Kanokjaruvijit K. Flow characteristics and heat transfer performances of a semi-confined impinging array of jets, effect of nozzle geometry. *Int J Heat Mass Transfer.* 2005;48(3-4):691-701.
25. Goodro M, Park J, Ligrani P, Fox M, Moon H-K. Effects of Mach number and Reynolds number on jet array impingement heat transfer. *Int J Heat Mass Transfer.* 2007;50:367-380.
26. Xing Y, Spring S, Weigand B. Experimental and numerical investigation of heat transfer characteristics of inline and staggered arrays of impinging jets. *ASME J Heat Transfer.* 2010;132(9):092201.
27. Chambers AC, Gillespie DR, Ireland PT, Kingston R. Enhancement of impingement cooling in a high cross-flow channel using shaped impingement cooling holes. *ASME J Turbomach.* 2010;132:021001.
28. Xing Y, Weigand B. Optimum jet-to-plate spacing of inline impingement heat transfer for different crossflow schemes. *ASME J Heat Transfer.* 2013;135:072201.
29. Culun P, Celik N, Pihtili K. Effects of design parameters on a multi-jet impinging heat transfer. *Alexandria Eng J.* 2018;57(4):4255-4266. [doi:10.1016/j.aej.2018.01.022](https://doi.org/10.1016/j.aej.2018.01.022)
30. Tepe AÜ, Yetişken Y, Uysal Ü, Arslan K. Experimental and numerical investigation of jet impingement cooling using extended jet holes. *Int J Heat Mass Transfer.* 2020;158:119945. [doi:10.1016/j.ijheatmasstransfer.2020.119945](https://doi.org/10.1016/j.ijheatmasstransfer.2020.119945)
31. Cai L, Wei X, Guo J. A new method to enhance the impingement/effusion cooling performance: applying a guiding ring to the hot side. *Proc Inst Mech Eng Part A: J Power Energy.* 2019;233(2):199-210. [doi:10.1177/0957650918779960](https://doi.org/10.1177/0957650918779960)
32. Hollworth BR, Dagan L. Arrays of impinging jets with spent fluid removal through vent holes on the target surface—part 1: average heat transfer. *ASME J Eng Power.* 1980;102(4):994-999.
33. Huber AM, Viskanta R. Comparison of convective heat transfer to perimeter and center jets in a confined impinging array of axisymmetric air jets. *Int J Heat Mass Transfer.* 1994;37(18):3025-3030.
34. Viskanta R, Huber AM. *Convective heat transfer to a confined impinging array of air jets with spent air exits.* 1994. <http://heattransfer.asmedigitalcollection.asme.org/> <https://doi.org/10.1115/1.2910908>

35. Cho HH, Rhee DH. Local heat/mass transfer measurement on the effusion plate in impingement/effusion cooling systems. *ASME J Turbomach.* 2001;123(3):601-608.
36. Rhee DH, Choi JH, Cho HH. Flow and heat (mass) transfer characteristics in an impingement/effusion cooling system with crossflow. *ASME J Turbomach.* 2003;125(1):74-82.
37. Cho HH, Rhee DH, Goldstein RJ. Effects of hole arrangements on local heat/mass transfer for Impingement/Effusion cooling with small hole spacing. *ASME J Turbomach.* 2008;130(4):041003.
38. Hong SK, Lee DH, Cho HH. Effect of jet direction on heat/mass transfer of rotating impingement jet. *Appl Therm Eng.* 2009;29(14-15):2914-2920.
39. Chang SW, Liou HF. Heat transfer of impinging jet-array onto concave- and convex-dimpled surfaces with effusion. *Int J Heat Mass Transfer.* 2009;52(19-20):4484-4499.
40. Onstad AJ, Elkins CJ, Moffat RJ, Eaton JK. Full-field flow measurements and heat transfer of a compact jet impingement array with local extraction of spent fluid. *ASME J Heat Transfer.* 2009;131(8):082201.
41. Chiu HC, Jang JH, Yan WM. Experimental study on the heat transfer under impinging elliptic jet array along a film hole surface using liquid crystal thermography. *Int J Heat Mass Transfer.* 2009;52(19-20):4650-4658.
42. Hoberg TB, Onstad AJ, Eaton JK. Heat transfer measurements for jet impingement arrays with local extraction. *Int J Heat Fluid Flow.* 2010;31(3):460-467.
43. Kim SH, Ahn KH, Park JS, Jung EY, Hwang KY, Cho HH. Local heat and mass transfer measurements for multi-layered impingement/effusion cooling: effects of pin spacing on the impingement and effusion plate. *Int J Heat Mass Transfer.* 2017;105:712-722. doi:10.1016/j.ijheatmasstransfer.2016.10.007
44. Ekkad SV, Huang Y, Han JC. Impingement heat transfer on a target plate with film cooling holes. *J Thermophys Heat Transfer.* 1999;13(4):522-528.
45. Miao JM, Wu CY. Numerical approach to hole shape effect on film cooling effectiveness over flat plate including internal impingement cooling chamber. *Int J Heat Mass Transfer.* 2006;49(5-6):919-938.
46. Oh SH, Lee DH, Kim KM, Kim MY, Cho H. Enhanced cooling effectiveness in full-coverage film cooling system with impingement jets. In: *ASME Turbo Expo, GT2008-50784.* American Society of Mechanical Engineers (ASME); 2008.
47. Jingzhou Z, Hao X, Chengfeng Y. Numerical study of flow and heat transfer characteristics of impingement/effusion cooling. *Chin J Aeronaut.* 2009;22(4):343-348.
48. Jung EY, Lee DH, Oh SH, Kim KM, Cho HH. Total cooling effectiveness on a staggered full-coverage film cooling plate with impinging jet. In: *ASME Turbo Expo GT 2010-23725;* 2010.
49. Ghorab MG. Adiabatic and conjugate cooling effectiveness analysis of a new hybrid scheme. *Int J Therm Sci.* 2011;50(6):965-983.
50. Mensch A, Thole KA. Overall effectiveness of a blade endwall with jet impingement and film cooling. *ASME J Eng Gas Turbines Power.* 2013;136(3):1-10.
51. Kosarev VF, Klinkov SV, Zaikovskii VN. Gas dynamics of a supersonic radial jet. Part II. *Thermophys Aeromech.* 2016;23(3):311-318.
52. Yang X, Liu Z, Liu Z, Wu B, Feng Z. Influence of jet impingement configurations and aerothermal variables on film cooling; 2016. <http://www.asme.org/about-asme/terms-of-use>
53. Luikov A. Conjugate convective heat transfer problems. *Int J Heat Mass Transfer.* 1974;17:257-265.
54. Prasad BVSSS, Sarkar SD. Conjugate laminar forced convection from a flat plate with imposed pressure gradient. *ASME J Heat Transfer.* 1993;115:469-472.
55. Sweeney PC, Rhodes JF. An infrared technique for evaluating turbine airfoil cooling designs. *ASME J Turbomach.* 2000;122(1):170-177.
56. Yang Y-T, Tsai SY. Numerical study of transient conjugate heat transfer of a turbulent impinging jet. *Int J Heat Mass Transfer.* 2007;50(5-6):799-807.
57. Panda RK, Prasad BVSSS. Conjugate heat transfer from an impingement and film-cooled flat plate. *J Thermophys Heat Transfer.* 2014;28(4):647-666.
58. Guo Q, Wen Z, Dou R. Experimental and numerical study on the transient heat-transfer characteristics of circular air jet impingement on a flat plate. *Int J Heat Mass Transfer.* 2017;104:1177-1188.
59. Devaraj K, Ganesh N. Conjugate heat transfer analysis of flat plate subjected to impingement and film cooling. *Int J Res Appl Sci Eng Technol.* 2021;9(9):1667-1678. doi:10.22214/ijraset.2021.38214

60. Chupp RE, Helms HE, McFadden PW. Evaluation of internal heat-transfer coefficients for impingement-cooled turbine airfoils. *J Aircr.* 1969;6:203-208.
61. Metzger DE, Yamashita T, Jenkins CW. Impingement cooling of concave surfaces with lines of circular air jets. *J Eng Power.* 1969;91(3):149-155. <http://asme.org/terms>
62. Tabakoff W, Clevenger W. Gas turbine blade heat transfer augmentation by impingement of air jets having various configurations. *ASME J Eng Gas Turbines Power.* 1972;94:51-58.
63. Metzger DE, Takeuchi DI, Kuenstler PA. Effectiveness and heat transfer with full-coverage film cooling. *ASME J Eng Power.* 1973;95(3):180-184.
64. Hrycak P. Heat transfer from a row of impinging jets to concave cylindrical surfaces. *Int J Heat Mass Transfer.* 1981;24:407-419.
65. Bunker R, Metzger D. Local heat transfer in internally cooled turbine airfoil leading edge regions: part I—impingement cooling without film coolant extraction. *ASME J Turbomach.* 1990;112:451-458.
66. Taslim ME, Pan Y, Spring S. An experimental study of impingement on roughened airfoil leading-edge walls with film holes. In: *ASME Turbo Expo 2001;* 2001. <http://www.asme.org/about-asme/terms-of-use>
67. Nirmalan NV, Bunker RS, Hedlund CR. The measurement of full-surface internal heat transfer coefficients for turbine airfoils using a nondestructive thermal inertia technique. *ASME J Turbomach.* 2003;125(1):83-89.
68. Iacovides H, Kounadis D, Launder BE, Li J, Xu Z. Experimental study of the flow and thermal development of a row of cooling jets impinging on a rotating concave surface. *ASME J Turbomach.* 2005;127(1):222-229.
69. Fregeau M, Saeed F, Paraschivoiu I. Numerical heat transfer correlation for array of hot-air jets impinging on 3-dimensional concave surface. *J Aircr.* 2005;42:665-670.
70. Ibrahim MB, Kochuparambil BJ, Ekkad SV, Simon TW. CFD for jet impingement heat transfer with single jets and arrays. *ASME Turbo Expo.* American Society of Mechanical Engineers (ASME); 2005;2005: 359-373.
71. Fenot M, Dorignac E, Vullierme JJ. An experimental study on hot round jets impinging a concave surface. *Int J Heat Fluid Flow.* 2008;29(4):945-956.
72. Hong SK, Lee DH, Cho HH. Heat/mass transfer measurement on concave surface in rotating jet impingement. *J Mech Sci Technol.* 2008;22(10):1952-1958.
73. Kumar BVNR, Prasad BVSSS. Computational flow and heat transfer of a row of circular jets impinging on a concave surface. *Heat and Mass Transfer.* 2008;44(6):667-678.
74. Craft TJ, Iacovides H, Mostafa NA. Modelling of three-dimensional jet array impingement and heat transfer on a concave surface. *Int J Heat Fluid Flow.* 2008;29(3):687-702.
75. Jung EY, Park CU, Lee DH, Kim KM, Cho HH. Effect of the injection angle on local heat transfer in a showerhead cooling with array impingement jets. *Int J Therm Sci.* 2018;124:344-355. doi:[10.1016/j.ijthermalsci.2017.10.033](https://doi.org/10.1016/j.ijthermalsci.2017.10.033)
76. Bolek A, Bayraktar S. Flow and heat transfer investigation of a circular jet issuing on different types of surfaces. *Sādhanā.* 2019;44:1-11. doi:[10.1007/s12046-019-1226-6](https://doi.org/10.1007/s12046-019-1226-6)
77. Metzger DE, Bunker RS. Local heat transfer in internally cooled turbine airfoil leading edge regions: part II—impingement cooling with film coolant extraction. *ASME J Turbomach.* 1990;112(3):459-466.
78. Taslim ME, Setayeshgar L, Spring SD. An experimental evaluation of advanced leading edge impingement cooling concepts. *J Turbomach.* 2001;123(1):147-153. doi:[10.1115/1.1331537](https://doi.org/10.1115/1.1331537)
79. Taslim ME, Khanicheh A. Experimental and numerical study of impingement on an airfoil leading edge with and without showerhead and gill film holes. *J Turbomach.* 2006;128(2):310-320. doi:[10.1115/1.2137742](https://doi.org/10.1115/1.2137742)
80. Ashok Kumar M, Prasad BVSSS. Computational investigations of impingement heat transfer on an effused concave surface. *Int J Fluid Mach Syst.* 2012;5(2):72-90. doi:[10.5293/IJFMS.2012.5.2.072](https://doi.org/10.5293/IJFMS.2012.5.2.072)
81. Albert JE, Bogard DG, Cunha F. Adiabatic and overall effectiveness for a film cooled blade. *ASME Turbo Expo.* 2004;2:251-259.
82. Kusterer K, Bohn D, Sugimoto T, Tanaka R. Conjugate heat transfer analysis of a test configuration for a film-cooled blade. In: *Proceedings of the International Gas Turbine Congress, TS-083;* 2003.

83. Kusterer K, Hagedorn T, Bohn D, Sugimoto T, Tanaka R. Improvement of a film-cooled blade by application of the conjugate calculation technique. In: Bogard DG, ed. *ASME J Turbomach*. American Society of Mechanical Engineers (ASME); 2006;128(3):572-578.
84. Ravelli S, Dobrowolski L, Bogard DG. Evaluating the effects of internal impingement cooling on a film cooled turbine blade leading edge. *ASME Turbo Expo*. 2010;2010:1655-1665.
85. Nathan ML, Dyson TE, Bogard DG, Bradshaw SD. Adiabatic and overall effectiveness for the showerhead film cooling of a turbine vane. In: *ASME Turbo Expo, GT2012-69109*; 2012:1537-1547. <https://doi.org/10.1115/GT2012-69109>
86. Montomoli F, Massini M, Yang H, Han JC. The benefit of high-conductivity materials in film cooled turbine nozzles. *Int J Heat Fluid Flow*. 2012;34:107-116.
87. Chandran D, Prasad BVSSS. Conjugate heat transfer study of combined impingement and showerhead film cooling near NGV leading edge. *Int J Rotating Mach*. 2015.
88. Lamani S. Conjugate heat transfer analysis of jet impingement and film cooling on leading edge of gas turbine blade. *Int J Innovations Eng Res Technol*. 2017;4.
89. Heidmann JD, Kassab AJ, Divo EA, Rodriguez F, Steinthorsson E. Conjugate heat transfer effects on a realistic film-cooled turbine vane. In: *Proceedings of the ASME Turbo Expo, GT2003-38553*; 2003;5: 361-371. <https://doi.org/10.1115/GT2003-38553>
90. Mazur Z, Hernández-Rossette A, García-Illescas R, Luna-Ramírez A. Analysis of conjugate heat transfer of a gas turbine first stage nozzle. *Appl Therm Eng*. 2006;26(16):1796-1806.
91. Dees JE, Bogard DG, Ledezma GA, Laskowski GM. Overall and adiabatic effectiveness values on a scaled-up, simulated gas turbine vane. *J Turbomach*. 2013;135(3). doi:[10.1115/1.4023105](https://doi.org/10.1115/1.4023105)
92. Dees JE, Bogard DG, Ledezma GA, Laskowski GM, Tolpadi AK. Experimental measurements and computational predictions for an internally cooled simulated turbine vane. *ASME J Turbomach*. 2012;134(061003):1-9.
93. Albert JE, Bogard DG. Experimental simulation of contaminant deposition on a film-cooled turbine vane pressure side with a trench. *ASME J Turbomach*. 2013;135(5):051008.
94. Williams RP, Dyson TE, Bogard DG, Bradshaw SD. Sensitivity of the overall effectiveness to film cooling and internal cooling on a turbine vane suction side. *ASME J Turbomach*. 2014;136:031006.
95. Pujari AK, Prasad BVSSS, Sitaram N. Conjugate heat transfer analysis on the interior surface of nozzle guide vane with combined impingement and film cooling. *Int J Turbo Jet Engines*. 2017. doi:[10.1515/tjj-2017-0026](https://doi.org/10.1515/tjj-2017-0026)
96. Pujari AK, Prasad BVSSS, Sitaram N. Effect of thermal conductivity on nozzle guide vane internal surface temperature distribution. *Int J Turbo Jet Engines*. 2018. doi:[10.1515/tjj-2017-0061](https://doi.org/10.1515/tjj-2017-0061)
97. Pujari AK. CFD study of combined impingement and film cooling flow on the internal surface temperature distribution of a vane. *Int J Turbo Jet Engines*. 2019. doi:[10.1515/tjj-2019-0010](https://doi.org/10.1515/tjj-2019-0010)
98. Wu Z, Laurence D, Iacovides H, Afgan I. Direct simulation of conjugate heat transfer of jet in channel crossflow. *Int J Heat Mass Transfer*. 2017;110:193-208. doi:[10.1016/j.ijheatmasstransfer.2017.03.027](https://doi.org/10.1016/j.ijheatmasstransfer.2017.03.027)
99. Parsons JA, Han JC. Rotation effect on jet impingement heat transfer in smooth rectangular channels with radially outward crossflow. *Int J Heat Mass Transfer*. 1998;41(13):2059-2071.
100. Parsons JA, Han JC, Lee CP. Rotation effect on jet impingement heat transfer in smooth rectangular channels with four heated walls and radially outward crossflow. *ASME J Turbomach*. 1998;120(1):79-85.
101. Akella K, Han JC. Jet impingement cooling in rotating two-pass rectangular channels with smooth walls. *AIAA J Thermophys Heat Transfer*. 1998;12(4):582-588.
102. Akella K, Han JC. Impingement cooling in rotating Two-Pass rectangular channels with ribbed target walls. *AIAA J Thermophys Heat Transfer*. 1999;13(3):364-371.
103. Parsons JA, Han JC. Rotation effect on jet impingement heat transfer in smooth rectangular channels with film coolant extraction. *Int J Rotating Mach*. 2001;7(2):87-103.
104. Parsons JA, Han JC. Jet impingement heat transfer in rotating channels with staggered extraction flow. *AIAA J Thermophys Heat Transfer*. 2005;19(2):156-162.
105. Azad GMS, Huang Y, Han JC. Jet impingement heat transfer on dimpled surfaces using a transient liquid crystal technique. *AIAA J Thermophys Heat Transfer*. 2000;14(2):186-193.
106. Azad GMS, Huang Y, Han JC. Jet impingement heat transfer on pinned surfaces using a transient liquid crystal technique. *Int J Rotating Mach*. 2002;8(3):161-173.

107. Rallabandi AP, Rhee DH, Gao Z, Han JC. Heat transfer enhancement in rectangular channels with axial ribs or porous foam under through flow and impinging jet conditions. *Int J Heat Mass Transfer.* 2010;53(21-22):4663-4671. doi:[10.1016/j.ijheatmasstransfer.2010.06.027](https://doi.org/10.1016/j.ijheatmasstransfer.2010.06.027)
108. Mhetras S, Han JC, Huth M. Impingement heat transfer from jet arrays on turbulated target walls at large Reynolds numbers. *J Therm Sci Eng Appl.* 2013;6(2):021003. doi:[10.1115/1.4025665](https://doi.org/10.1115/1.4025665)

How to cite this article: Babji G, Pujari AK. Flow and heat transfer studies of multijet impingement cooling for different configurations: a review. *Heat Transfer.* 2022;1-69. doi:[10.1002/htj.22757](https://doi.org/10.1002/htj.22757)